2-8-2022

ADVANCING THE DEVELOPMENT OF ADDITIVELY MANUFACTURED SEQUENTIALLY CURED INTERPENETRATING POLYMER NETWORKS

Rachael J. Ross
Rowan University

ADVANCING THE DEVELOPMENT OF ADDITIVELY MANUFACTURED SEQUENTIALLY CURED INTERPENETRATING POLYMER NETWORKS

by

Rachael J. Ross

A Thesis

Submitted to the
Department of Chemical Engineering
College of Engineering
In partial fulfillment of the requirement
For the degree of
Master of Science in Chemical Engineering
At
Rowan University
January 7, 2022

Thesis Chair: Joseph F. Stanzione III, Ph.D.

Committee Members:
Alexander W. Bassett, Ph.D.
James A. Newell, Ph.D.
Jianwei Tu, Ph.D.

Dedications

For Mom and Dad – Thank you for helping me in every aspect to help me achieve all my goals and always believing in me. I would have never made it here without you.

Acknowledgements

I would like to thank my advisor Dr. Joseph F. Stanzione III for allowing me this great opportunity to pursue my graduate degree at Rowan University. Without him and this program I would not have been able to make the connections that I have formed and achieve the level of critical thinking that working at the Advanced Materials & Manufacturing Institute has taught me. It is because of him that I have infinitely expanded the number of possibilities for me and my beginning career.

Thank you to everyone working in Stanzione's Materials Research Lab for your support and collaboration for the last year and a half. I particularly would like to thank Dr. Alexander Bassett for acquainting me with the practices in the lab and allowing me to expand on his graduate work. I would also like to thank my fellow lab mates Alexandra Chong, Margaret Gillan, Jasmin Vasquez, John Chea, Tristan Bacha, Amit Dhundi, and Matthew Schwenger for the encouragement both in and out of group meetings. Without everyone, my experience completing my master's would not have been as enjoyable or successful, especially during a pandemic.

Finally, I'd like to thank my family and friends for helping me during this time. The last two years have been the most challenging of my life and I would not have been able to do it without such a strong support system.

Abstract

Rachael J. Ross
ADVANCING THE DEVELOPMENT OF ADDITIVELY MANUFACTURED
SEQUENTIALLY CURED INTERPENETRATING POLYMER NETWORKS
2021-2022
Joseph F. Stanzione, III, Ph.D.
Master of Science in Chemical Engineering

Recently vat photopolymerization (VPP), a type of additive manufacturing (AM), has the potential to be used for a variety of commercial and military applications due to the ability to make custom parts rapidly and with complex geometries. Many commercially available photopolymerizable resins consist of (meth)acrylate and epoxy functionality to ensure rapid cure time and minimal shrinkage. Today, researchers continue to find the optimal balance of (meth)acrylate/epoxy functionality in unique formulations and network configurations, such as interpenetrating polymer networks (IPN)s, to enhance processibility and the quality of the final printed part.

This work explores the structure-property relationships of a set of VPP resins synthesized from select starting materials in addition to improving the one-pot, two-step reaction methodology that has been employed by the Sustainable Materials Research Laboratory (SMRL) at Rowan University. Epoxy-methacrylate IPNs were prepared via a sequentially cured AM technique and subsequently evaluated for their thermal and mechanical properties. Through the incorporation of higher degrees of aliphatic character, the 3D printed IPNs yield an enhancement in toughness while maintaining thermal properties. Resultant IPNs were found to maintain glass transition temperatures above 130 ºC (tan δ) and increase fracture energies by more than 160%.

Table of Contents

Table of Contents (Continued)

Table of Contents (Continued)

List of Figures

List of Figures (Continued)

List of Tables

xi

List of Tables (Continued)

Chapter 1

Introduction

1.1 Overview

A constant goal in manufacturing is to make products faster and cheaper with better performance capabilities. In the interest of satisfying these goals, additive manufacturing (AM) has rapidly improved to accommodate major gains in productivity, substantial savings in cost, and improved product quality particularly in the field of synthetic polymers. Polymers are used extensively around the globe in automotive, aerospace, computer, biomedical, military applications, and others due to economic advantages and durability. With such a large consumer base, polymers are a popular area of interest among researchers and chemical engineers to further investigate how to manipulate network configurations, syntheses parameters, and functionalities to achieve higher performing polymers. This work aims to evaluate the effect of different functionalities of an established interpenetrating polymer network (IPN) that is cured via AM. Additionally, this work altered the proposed reaction schema used to synthesize the IPN to satisfy the continuous evolvement of industry trends. This chapter introduces the general concepts behind AM and key monomer configurations to consider when synthesizing high performance polymers with relatively high moduli (>2 GPa), T_gs ($\geq$ 120 $^{\mathrm{o}}$C) and adequate fracture toughness ($G_{IC} \approx$ 200-250 J m^{-2}).

1.2 Additive Manufacturing

Additive manufacturing (AM) is a technique that simply means to build or improve materials by addition. While this idea has been around for over 10,000 years

when homes were built brick by brick, the oldest patent for AM techniques was not recorded until 1890 by Blanther for making topographical relief maps [1]–[3]. As time progresses and technology continues to advance, AM processes have grown from ancient construction strategies to a market worth over $12 billion USD in 2020 [4], [5]. Most of this growth has taken place over the last 30 years with the rapid improvement in technology and key market drivers that call for faster build times, reduced manufacturing costs, and more customized products [2]. Common examples of AM processes that aim to satisfy these market demands are ink jet printing, vat photopolymerization (VPP), injection molding, directed energy deposition and selective laser melting [1].

Traditional machining techniques, otherwise known as subtractive manufacturing methods, require a bulk material and removes pieces, or chips, to make the desired product or model. This difference alone is enough to sway most manufacturers and engineers towards AM as a means of producing materials due to reducing costs and energy to fabricate products. But there are additional reasons why AM has taken precedence over traditional manufacturing techniques. Aside from being less wasteful AM offers more precision during the fabrication process to produce more complex geometries [6]. Unlike subtractive manufacturing, which requires a block of finished material to then shape into the finished prototype, AM can change the final properties of the material with the proper optimization of various parameters such as exposure times and printing speeds, to fulfill different functional requirements [1].

1.2.1 Vat Photopolymerization

The exclusive AM technique used throughout this work was stereolithography (SLA) which is a type of vat photopolymerization (VPP). SLA was chosen as the exclusive VPP method due to the ability of SLA to produce parts that are effectively isotropic [7], [8]. This technology, which is commonly referred to as 3D printing, was originally patented by Charles Hull of 3D Systems in 1986. Hull and collaborators combined computers, lasers, and principles of photochemistry to make commercial products at faster speeds. While initially used for small scale prototypes, SLA has grown to be frequently used in medical imaging, communication tools, and soft tool prototyping [9]. Despite rapid growth in the market, the basic operating principles of SLA have remained largely unchanged since 1991. Samples are fabricated in a layer-wise method where a laser selectively scans over the surface of a build platform that is submerged in a vat of photopolymerizable resin. Once a layer is fully formed, the build platform is then lifted vertically out of the vat to allow the resin to backfill, and the build platform is then submerged again for the fabrication of the following layer [1], [6], [9]. After all the layers are formed, the build platform and green polymer are lifted out of the vat and ready for subsequent post processing steps. Oftentimes, the manufactured part is separated from the build platform, washed to remove any uncured resin, and polished before final application [6].

1.2.2 Vat Photopolymerization Resins

Currently, most commercial SLA resins have a viscosity between 500-1500 cP at 25 ^{o}C and must cure a single layer from 15-300 s [10]. To accommodate these

3

requirements, scientists must consider reaction rates and the ability of the resin to flow easily. Typical commercial resin formulations for SLA applications are a mixture of oligomers, monomers, and photoinitiators that are ready to use once opened. Most oligomers and monomers found in resin formulations are derived from polyols, epoxides, (meth) acrylic acids and their respective esters to create polyester acrylates, epoxy acrylates, urethane acrylates, amine acrylates, and cycloaliphatic epoxies. These functionalities provide cross-linking polymerization that is initiated via a photoinitiator. Common photoinitiators found in resin formulations are either free-radical photoinitiators and cationic polymerization photoinitiators. Generally, free-radical polymerization photoinitiators, namely benzoyl radicals, are used in SLA resins due to the wide range of photoinitiators readily available [6], [11]. While less frequently explored, many reviews have been written outlining the successes of cationic photopolymerization facilitated by onium salts or organometallic compounds [6], [12]–[14].

In some cases, a reactive diluent is added to a resin formulation to accommodate the lower viscosity requirements necessary for SLA. Reactive diluents are found in VPP resins in order to reduce viscosity but also limit any shrinking of the final printed part without affecting resin reactivity or stability [15]. While serving to reduce resin viscosity and improve printing properties, reactive diluents also reduce processing costs. Commonly used reactive diluents are methacrylated fatty acids, lignin based methacrylates, and HELOXY^{TM} modifiers [16], [17]. HELOXY^{TM} modifiers (HM) are mono-, di-, or poly- epoxy functionalized molecules that enable formulators to manipulate epoxy resin systems to accommodate different applications ranging from

consumer grade to military. Aside from reducing resin viscosity, HM may be used to reduce surface tension of a resin or modify different performance characteristics like flexibility and strength. Some commonly used modifiers are shown in Figure 1.

Figure 1

Chemical Structures of Commonly Used HELOXY^TM Modifiers

HELOXY Modifier 107

HELOXY Modifier 61

HELOXY Modifier 68

HELOXY Modifier 48
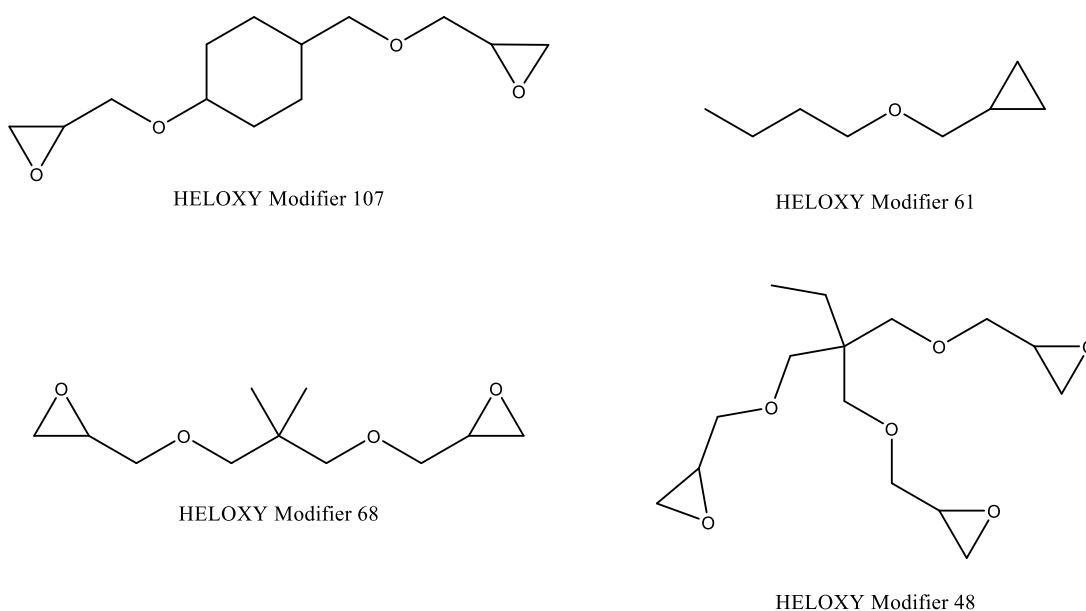
As early as 1989, different SLA resins were prepared with acrylate functionalities that exhibited high reactivity but weak parts from curling and shrinking [6], [18], [19]. These contrasted with epoxy based resin systems that were found to be more accurate and stronger than acrylate based resin systems due to negligible shrinkage, but had a much slower rate of reaction [6]. Due to the slow reaction rates, all epoxy-based resin systems designed for SLA must have some level of (meth)acrylate functionality.

When curing both (meth)acrylate networks and epoxy networks in the presence of one another, an IPN resin system formed. IPN resins synthesized with both (meth)acrylate and epoxy functionalities designed for SLA applications offer both the fast-curing speeds of (meth)acrylate functionalities with enhances in toughness and promoted adhesion characteristics often associated with epoxy-based resins. Finding the optimal balance between (meth)acrylate and epoxy functionalities in an IPN resin are still being extensively explored in the literature [20]–[24].

1.3 Polymer Design

1.3.1 Interpenetrating Polymer Networks

IPNs can be simply defined as when a material consists of at least two polymers in network form. This broad definition implies that an IPN occurs when two or more polymers have been synthesized and/or crosslinked in the presence of one another. IPNs do not dissolve in solvents and suppress both creep and flow which separates them from polymer blends, blocks, and grafts [25]. Studies around IPNs date as far back as 1914 when J. W Aylsworth added natural rubber and sulfur in an attempt to toughen the phenol-formaldehyde resin known as Bakelite [25], [26]. After Aylsworth's work, many efforts were made to continuously understand the various characteristics of polymer materials and a few patents on IPNs were issued. Despite decent advancements regarding IPNs, the actual term IPN was not introduced until 1960 when John Millar conducted his work on polystyrene IPNs as ion-exchange resin matrices [25], [27], [28].

Significant advancements have been made by researchers to master the fundamental ideas and principles behind IPNs since the work performed by John Millar

[25]. IPNs are often chosen over IPNs can be divided according to the way in which the chemical networks are formed. Simultaneous interpenetrating polymer networks (SINs) are known as the formation of two or more polymer networks in the presence of one another at the same time by noninterfering modes of polymerization. Sequentially cured IPNs are characterized by the formation of each network within the material forming independently of one another. In other words, the first monomer of the network is synthesized and becomes crosslinked Polymer I. The second monomer, as well as initiator and crosslinking agent, then swells within the Polymer I and is polymerized *in situ* [25]. Both simultaneously cured and sequentially cure IPNs have been well synthesized and observed over the last 60 years. Among some of the commonly studied IPNs are acrylate/methacrylate-epoxy IPNs [24], [29]–[32]. These systems offer more versatility than other IPN systems due to the different curing mechanisms per each polymer network. The acrylate/methacrylate network cures via free-radical polymerization with an appropriate photoinitiator, which is prompted via light and often associated with rapid curing speeds but considerable shrinkage of the polymer. The epoxy network can cure with a curing agent consisting of either amines or anhydrides with the aid of elevated temperatures which while characterized with a slower curing mechanism offers minimal shrinkage of the final cured polymer [33]. The diversity in curing mechanisms allows for the option to cure simultaneously or sequentially depending on the intended polymer properties.

For the work presented in this thesis, sequentially cured methacrylate-epoxy IPNs were investigated to study the relationships between chemical functionality and polymer

7

properties. IPNs were chosen over vinyl ester resins (VERs), epoxy-based resins, and traditional thermoplastics due to the ability of an IPN to be cured via SLA and the opportunity for synthesizing high performance materials. A visual representation for each polymer network formed during each curing step is shown in Figure 2.

Figure 2

Visual Representation of a) Neat Resin with Curing Agent b) Green-Cured Polymer After SLA Step c) Fully Cured Polymer After Subsequent Post-Processing Steps
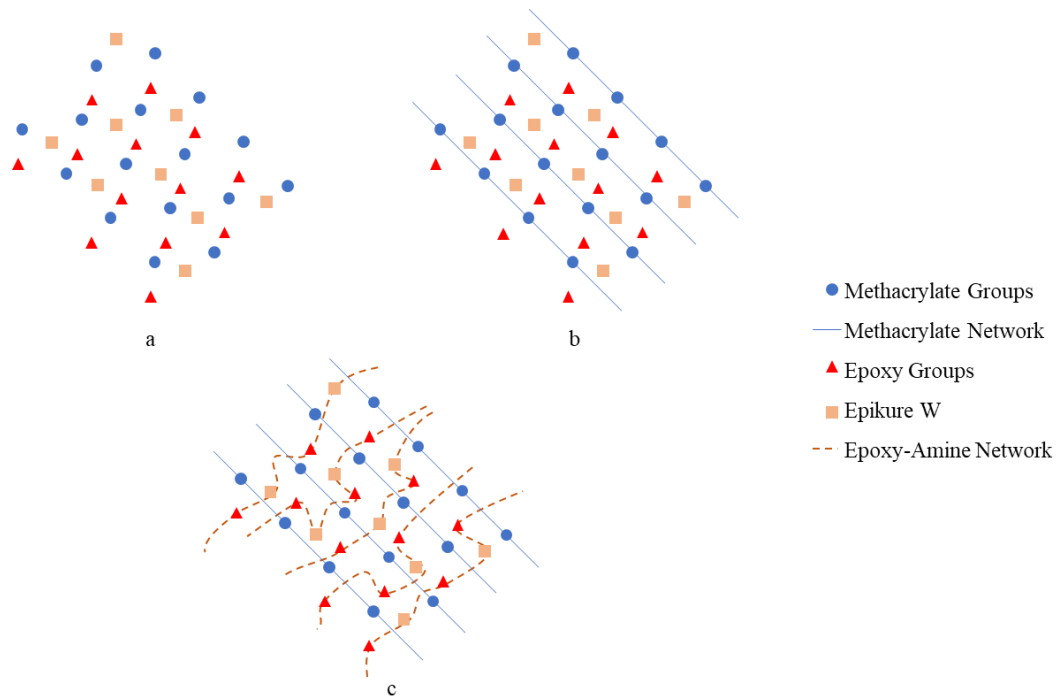
Due to the multicomponent system within IPNs, a certain degree of phase separation can be observed due to the incompatibility between polymer networks. The

dual-crosslinked nature of IPNs greatly controls the size, shape, and composition of each

phase domain within an IPN which controls the final polymer properties such as glass

transition temperatures and impact resistance [25]. The existence of the multicomponent

system already increases the toughness of a material which makes IPNs a great area of

interest for biomedical materials, vibration damping materials, and AM applications

[34]–[40].

1.3.2   *Chemical Structure & Polymer Properties*

Controlling polymer properties can be done by optimizing processing

parameters via curing methods and polymerization mechanisms or by finding the perfect

balance between epoxy and methacrylate modalities in a monomer or IPN. Taking a

closer look into the polymer or monomer structure can also aid in predicting the final

properties of a polymer. Polymers can be divided across a wide variety of subdivisions

ranging from the way they are polymerized, structured, and assembled [41]. More

specifically, a polymer can be characterized based on the nature the carbon and hydrogen

atoms are arranged throughout the system. Hydrocarbons can be described as either

aliphatic or aromatic in nature. Typically, the primary difference between aliphatic and

aromatic compounds is the presence of a benzene ring, which is when 6 carbons are

connected by conjugated π-bonds within a ring [41]. This key difference affects the

nature of the monomer and polymer significantly. Regarding polymer performance,

higher degrees of aromatic content result in a more rigid polymer with higher glass

transition temperatures (T_g). Conversely, higher degrees of aliphatic content allude to a

more flexible polymer that is more resist to impact with a lower T_g [42]–[44]. This may

be due to the ability of aliphatic carbons to react more freely due to lack of electron delocalization [41]. Considering the benefits of both aromatic and aliphatic character on final polymer properties can yield significant advantages.

1.4 Thesis Summary

This thesis explores how different chemical structures of monomers can impact polymer properties in IPN systems that are used in resins for SLA applications in an established one-pot-two-step methodology. This hypothesis of this thesis states that by introducing a higher degree of aliphatic character to IPNs, a commercially relevant resin for SLA can be made that will maintain thermal properties while improving mechanical strength and improving processing parameters. To illustrate this theory, the recently developed IPN thermoset consisting of both vinyl-ester and epoxy-amine components, PMEM828 by Bassett et. al was chosen as the base resin system [34]. Chapter 2 explains the analytical techniques and instrumentation involved in this work. Chapter 3 lists the experimental methods and materials used to synthesize each resin, prepare the IPN, and characterize the final polymer properties. The results and discussion of all analytical, thermal, and mechanical properties for each iteration of AM polymers are provided in Chapter 4. Chapter 5 presents conclusions and recommendations for future work beyond the scope of this thesis.

Chapter 2

Characterization Methods

2.1 Introduction

This chapter introduces each method utilized to characterize the resins and respective printed polymers studied in this work. This section includes nuclear magnetic resonance (NMR) spectroscopy, rheology, Fourier transform infrared (FTIR) spectroscopy, density measurements, differential scanning calorimetry (DSC), thermogravimetric analysis (TGA), dynamic mechanical analysis (DMA), compression testing, fracture toughness, and *t*-tests. Each characterization technique will be described with a brief history, general concepts, and theories in their respective sections. Experimental methods specific to this work will be discussed further in Chapter 3.

2.2 Nuclear Magnetic Resonance (NMR) Spectroscopy

Nuclear Magnetic Resonance (NMR) spectroscopy is a valuable spectroscopic technique used to investigate the molecular structure and molecular processes of various organic compounds [45]–[47]. The first developments in NMR were carried out by researchers Bloch and Purcell in 1945 [45], [48]. However. the importance of NMR did not become relevant until 1949 where the effect of the chemical shift was discovered, and chemical applications could be achieved. Bloch and Purcell eventually won the Nobel Prize in Physics for the significance of NMR in 1952, which was right before the appearance of the first commercial NMR in 1953 [45]. Today, due to the major advancements in technology surrounding superconducting magnets and liquid cooling

11

systems, NMR has become one of the most powerful techniques used by researchers to study chemical structure [41]. A variety of different nuclei can be studied with NMR including ^{1}H, ^{13}C, ^{15}N, ^{19}F, and ^{31}P. For this work, only ^{1}H nuclei were examined to determine the chemical structure of investigated polymers.

^{1}H-NMR spectroscopy is performed by applying a very strong magnetic field and source of radiation to a sample. This allows researchers to study the interaction between electromagnetic radiation and the nuclei within the hydrogen atoms of a sample with the spectrum produced from ^{1}H-NMR. The ^{1}H-NMR spectra reveals the response, or magnetic resonance, of ^{1}H nuclei to show the proximity of the nuclei to other atomic nuclei, electronegative atoms, and double bonds in the chemical structure of the sample [48]. These responses are then compared to a reference peak from an inert chemical, which is typically tetramethylsilane (TMS), to determine the location, area, and shape of each ^{1}H signal. The proximity of the nuclei to other atomic nuclei and electronegative atoms will be indicated by the location, or chemical shift (ppm), of each proton signal on the ^{1}H-NMR spectrum. The area and shape of each ^{1}H signal will correspond to the number of protons representative of a given peak and the number of neighboring ^{1}H respectively [41]. ^{1}H-NMR spectroscopy was performed on a 400 MHz Varian NMR (32 scans at 298K) to evaluate changes in chemical structure over time, which is discussed further in Chapter 4.

2.3 Rheology

Rheology was first defined by Professor Bingham of Lafayette College in Indiana as the study of the deformation and flow of matter in 1929 [49]. Viscosity is

defined as the measure of resistance to flow due to internal friction between layers of fluid [50]. Rheological techniques are oftentimes used to determine the viscosity of liquids which over the years has become an important parameter to various chemical processing industries. Rheological instruments will apply different levels of force, or shear, at different speeds to determine the viscosity of a liquid by measuring the response of the sample. The response is measured as a shear stress as a function of shear rate. When the ratio of shear stress to shear rate is constant the liquid is determined to be Newtonian due to Newton's hypothesis. Newton hypothesized that the internal friction is directly proportional to the relative velocity of fluid particles displaying a linear relationship between shear stress and shear rate known as viscosity [51]. Fluids that do not exhibit a constant viscosity over different shear rates are deemed Non-Newtonian [50]. In this study, rheology measurements were determined with a TA Instruments Discovery HR-2 Rotational Rheometer. Specific operating procedures and equipment set up are further explained in Chapter 3.

2.4 Fourier Transform Infrared (FTIR) Spectroscopy

Infrared spectroscopy has been a widely used tool to analyze the nature of chemical bonds in both organic and inorganic materials since the 1950s [50], [52]. Fourier transform infrared (FTIR) spectroscopy was developed in the 1970s and quickly became the most popular spectroscopy tool among researchers due to its high sensitivity, quick turnaround, and non-destructive nature [53]. With IR spectroscopy, a sample is exposed to infrared radiation to determine the different chemical functionalities within its structure. Frequencies from the IR radiation are either absorbed or passed through the

sample at different wavelengths of light to determine characteristic bending, vibrations, or rotations of chemical bonds within a sample. These frequencies are presented in the form of an absorbency plot [41].

Different IR spectrometers will provide different absorbency plots but the most widely used IR spectrometer is an FTIR which uses the mathematical operation known as the Fourier Transform to manipulate the frequencies that pass through the sample to form a corresponding absorbency plot [41]. IR spectroscopy is divided into three separate ranges of wavelengths used to characterize the chemical structure of a sample. The three separate wavelengths are divided into far-IR at 200-10 cm^{-1}, mid-IR at 4000-200 cm^{-1}, and near-IR at 12,800-4000 cm^{-1} [54]. In this work, near-IR was employed to determine the extents of cure of each chemical functionality along different stages of the curing process for each synthesized IPN.

2.5 Density Measurements

In this thesis, density measurements were obtained for each cured IPN studied using Archimedes Principle [55]. Once fully cured, the weight of each polymer was found using a density kit and scale that measured the weight of the polymer in air and the weight of the polymer submerged in water. The density, ρ, was then calculated in accordance with Equation 1.

$$\rho = \left(\frac{W_{dry}}{W_{dry} - W_{wet}} \right) \times \rho_{water} \qquad (1)$$

Equation 1 calculates the density of the polymer using the weight of the polymer

in air designated by W_{dry}, the weight of the polymer submerged in water designated by

W_{wet} and the density of water (ρ_{water}) which is assumed to be 0.997 g/mL at 25°C [55].

All density measurements were performed in triplicate for each cured polymer. Density

measurements were then used to calculate the molecular weight between crosslinks in

tandem with results from dynamic mechanical analysis, which will be discussed in later

sections.

2.6 Differential Scanning Calorimetry (DSC)

Differential scanning calorimetry (DSC) is the most widely used analytical

technique to characterize the thermal analysis of various polymers. DSC evaluates the

heat flow rate, or differential power, of a given sample in an inert atmosphere (N_2) as a

function of temperature [50]. By measuring the differential power of a polymer, different

properties can be determined such as melting point (T_m), glass transition temperature (T_g),

degree of crystallinity, and degree of polymerization [33], [50].

DSC can be performed using two different types of instruments known as the

power compensation differential scanning calorimeter, and the heat flux calorimeter [50].

The work performed in this studied used a heat flux calorimeter which operates by

comparing two aluminum pans, one pan holding 5-10 mg of polymer sample and one

empty reference pan, in the same furnace. The furnace is programmed to ramp up to a

certain temperature at a specified rate. As the temperature increases, the temperature

difference between sample and reference pan are monitored with a thermocouple to

calculate the differential heat flow [50]. Significant changes in differential heat flow can correspond to different thermal transitions like the curing of a polymer. Typically, as a sample cures, more energy is released resulting in significant exothermic events [50]. In this work, DSC was used to observe if all polymers were fully cured by the presence or lack thereof significant exotherms.

2.7 Thermogravimetric Analysis (TGA)

Thermogravimetric analysis operates by measuring the change in weight of a specimen over a range of temperatures in either inert or oxidative environments [50]. Analyzing changes in mass of a polymer as a function of temperature allows researchers to identify different thermal events such as degradation, phase changes, and chemical reactions. This is done by measuring a small amount of sample into a platinum or ceramic pan that is then weighed continuously with an analytical balance in a programmed furnace [56]. Using TGA in combination with other thermal analysis techniques offers valuable insight into the chemical structure of different polymers [50].

In this work, TGA was employed to evaluate the different degradation properties of each synthesized polymer. Evaluating mass as a function of temperature determined the initial decomposition temperature (IDT), the temperature at 50% mass loss ($T_{50\%}$), and the final char content of the sample. The second derivative curve of the mass as a function of temperature revealed the maximum rate of degradation (T_{max}) of each investigated polymer.

16

2.8 Dynamic Mechanical Analysis (DMA)

Dynamic mechanical analysis (DMA) is an analytical tool used to capture the viscoelastic properties of various polymers [50]. The first reported DMA experiments conducted date back to 1909 by Poynting who was attempting to measure the elasticity of a material [57]. Over the next 50 years, DMA became an integral part of polymer science and the theories associated with DMA became more developed [57], [58]. Today, due to the rapid advancement of software and technology, many different types of dynamic mechanical analyzers exist on the market and are commonly found in polymer laboratories.

DMA can effectively illustrate both the elastic and viscous characteristics of various polymers. Different values found through DMA reveal information about polymer behavior in relation to stiffness, damping, glass transition temperature, vitrification, stress relaxation, and creep recovery [50], [57]. Different thermomechanical properties correspond to different types of deformation which can be achieved with a wide array of geometries used with DMA. Among the most commonly used geometries for DMA are ones associated with 3-point bending, clamped bending, compression, tension, and shear [50]. In this work, storage modulus (E'), loss modulus (E''), tan δ, and the effective molecular weight between crosslinks (M_c) was determined via a single-cantilever geometry which produces a clamped bending stress.

DMA quantifies the viscoelastic characteristics of a polymer by applying an oscillatory force to a sample and measuring the given response [50], [56], [57]. The response delay of the sample is quantified through a phase angle denoted δ as a function

17

of temperature [57]. Modulus, which provides insight to a materials resistance to deformation, is oftentimes measured as the slope of the stress-strain curve. In the instance of DMA, the complex modulus is found due to the oscillatory nature of the applied stress. The complex modulus can provide both the storage modulus *(E'),* which corresponds to the energy stored in the chemical bonds of a material, and the loss modulus *(E''),* which represents the amount of energy dissipated as heat from a viscous response [58]. Storage modulus *(E')* and loss modulus *(E'')* can be defined by Equations 2 and 3 respectively.

$$E' = \frac{\sigma_0}{\varepsilon_0} \cos(\delta) \tag{2}$$

$$E'' = \frac{\sigma_0}{\varepsilon_0} \sin(\delta) \tag{3}$$

Both moduli are determined by manipulating δ and multiplying it by the ratio between stress, σ_0 and strain, ε_0. Tan δ, which can yield information about damping properties, can be found as the ratio between E' and loss modulus E'' as shown in Equation 4 [57].

$$tan\delta = \frac{E''}{E'} \tag{4}$$

These values can be further manipulated to find the effective molecular weight between crosslinks *(M_c)* in accordance with the Theory of Rubber Elasticity as seen in Equation 5.

$$E = \frac{3RT\rho}{M_C} \tag{5}$$

This equation finds the M_c by using the minimum rubbery storage modulus *(E),* the ideal gas constant *(R),* the absolute rubbery temperature *(T),* and the density determined via Archimedes principle *(ρ)* [55].

2.9 Compression Testing

Compression testing was performed in this study to determine the compressive modulus of elasticity, as well as the maximum compressive strength. These values were found to describe the behavior of each polymer when subjected to compressive stress at a low and uniforms rate of loading [50]. Typically, when designing materials, compression testing will consider the results of impact, creep, and fatigue tests. This will consider the dependence of rigidity and strength of plastics when designing parts.

The most widely sought after values when performing compression testing are compressive strength and compressive modulus [50]. Compressive modulus will illustrate the stiffness of a material by representing the response of molecular chains within a polymer to deformation by translational movements from compression [59]. The compressive modulus can be found by assuming negligible barreling of a sample and following the same protocol for calculating Young's modulus. Young modulus is defined as shown in Equation 6.

$$E = \frac{\sigma}{\varepsilon} \tag{6}$$

To find Young's modulus, the compressive stress, σ, is divided by the compressive strain, ε, which is calculated as shown in Equation 7.

$$\varepsilon = \frac{\Delta L}{L_0} \tag{7}$$

This equation shows that compressive strain is calculated by finding the change in gauge length of the sample relative to the initial gauge length *(L_0)* of the sample. In this thesis, all compression testing was performed on an Instron 5966 mechanical tester with cylindrical samples prepared in accordance to ASTM D695-15 [60]. Further details associated with compression testing are discussed later in Chapter 3.

2.10 Fracture Testing

Fracture toughness is an important parameter for engineers to observe because of the additional knowledge of strengths and weaknesses characteristic of various studied materials [61]. The mechanical test method employed to determine fracture toughness for the investigated polymers in this work aimed to find the critical strain energy release rate *(G_{IC})* and critical-stress intensity factor *(K_{IC})* at fracture initiation. Two testing geometries are typically used when studying the deformation and fracture of plastic materials. Either a single-edge-notch bending (SENB) or a compact tension (CT) geometry can be employed. For the studies carried out in this work, a SENB geometry was used to determine the fracture properties of plastic specimens prepared in accordance to ASTM D5045-14 [62].

Generally, when investigating the fracture behavior of polymers, energy is absorbed within the sample by viscoelastic deformation of polymer chains and followed by the generation of new surface area. The generation of new surface area can be a result of energy absorption by shear yielding, crazing, or crack propagation [61][25]. Due to the

high speed at which a crack can propagate, the technique used to evaluate the fracture

behavior of different polymers is very sensitive [63]. Typically, tapping a razor blade into

a specimen is the preferred technique for crack propagation as it allows a natural crack to

spread throughout a sample. Other techniques can be used to initiate a crack depending

on the brittle nature of the material, including scoring with a razor blade, or inserting thin

pieces of film into samples during cure. While these techniques offer comparable fracture

data, they do not truly represent the actual fracture behavior of a polymer. For the

fracture analysis performed in this work, a scoring methodology was used to generate a

crack across the notch that was machined into each specimen. For relative toughness

comparisons, a scoring method can be used to illustrate the toughness between various

materials [63].

2.11 *t*-Test

A *t*-test is a statistical test performed to verify the significance between the mean

values of two sample sets [64]. A *t*-test checks whether a statistical hypothesis is correct

for samples with comparable variances assuming a normal distribution. In the case of

comparing two independent samples, an unpaired *t*-test can be performed to determine

whether the samples are statistically different from one another. An unpaired *t*-test can be

performed as shown in accordance with Equation 8.

$$t_p = \frac{|\bar{x}_1 - \bar{x}_2|}{s_d \sqrt{\dfrac{1}{n_1} + \dfrac{1}{n_2}}} \tag{8}$$

Equation 8 calculates the test value (t_p) where x_1 and x_2 are the means of sample set 1 and 2 respectively, s_d is the standard deviation, and n_1 and n_2 are the variable set size for each sample group [64]. Once the t_p is calculated a comparison must be made against the critical test value (t_{crit}) which can be found in Appendix A. If $t_p < t_{crit}$ then the difference between sample sets is found to be statistically insignificant. If $t_p \geq t_{crit}$ then the difference between sample sets is found to be statistically significant. All t-tests conducted in this work were performed with a 95% confidence level.

Chapter 3

Experimental Methods and Materials

3.1 Introduction

This chapter serves to outline the experimental materials, procedures, and methods used in this body of work. The synthesis of each resin system, the addition of curing agents, and the techniques used to characterize the properties of each formulation are described. The characterization techniques used to quantify the thermal and mechanical properties of each fully cured IPN are detailed.

3.2 Materials

Phenol (detached crystals, 99%) was purchased from Beantown Chemical Corporation (Hudson, NH, USA). Deuterated chloroform (CDCl$_3$, 99.8% d) used for NMR, hydroquinone (99%), and 4-dimethylaminopyridine (DMAP) (99%) were purchased from Acros Organics (Fair Lawn, NJ, USA). Methacrylic anhydride (94%) and 4-tert-butylphenol (99%) were purchased from Alfa Aesar (Haverhill, MA, USA). AMC-2 catalyst was purchased from AMPAC Fine Chemicals (Rancho Cordova, CA, USA). Sodium Hydroxide (1N) was purchased from Fischer Scientific (Hampton, NH, USA). Phenolphthalein Indicator, (0.5% (w/v) in 50% (v/v) alcohol, neutralized) was purchased from Ricca Chemical Company (Arlington, TX, USA). (Diphenyl(2,4,6-trimethylbenzoyl) phosphine oxide (TPO) was purchased from TCI (Tokyo, Japan). Isopropyl alcohol (IPA) was purchased from VWR (Radnor, PA, USA). Compressed nitrogen (N$_2$, 99.998%) and compressed argon (Ar, 99.999%) were purchased from

Airgas (Radnor, PA, USA). Epon Resin 828 (diglycidyl ether of bisphenol A, DGEBA, Epon828), HELOXY^TM Modifier 68 (diglycidyl ether of neopentyl glycol), and Epikure Curing Agent W (diethyl toluene diamine) were purchased from Hexion (Columbus, OH, USA). NX-2026 (3-pentadeca-dienyl-phenol) and NC-510 (n-pentadecylphenol) were provided by Cardolite Corporation (Bristol, PA, USA). All chemicals were used as received.

3.3 Resin Synthesis

PMEM828 was synthesized using a one-pot-two-step (1P2S) methodology as shown in Figure 4 [65], [66]. For step 1, a mixture of phenol (50.00 g) and DMAP (3.3 g) were combined in a sealed 3-neck round bottom flask using a magnetic stir bar. Once combined compressed argon was used to purge the reaction vessel for 10 minutes to create an inert atmosphere. Once purged, methacrylic anhydride (82.8 g) was added and the vessel was heated to 50-55 °C with continuous stirring. After 72 hours, ^{1}H-NMR was used to confirm the esterification of phenol and formation of methacrylic acid. After step 1, the reaction mixture was allowed to cool ambiently to room temperature. A stoichiometric amount of Epon828 (199.8 g) was then added to the vessel along with AMC-2 catalyst (0.2 g) and combined using a mechanical mixer. The vessel was then heated to 70-77°C and monitored via acid number titration until completion. Completion was determined by an acid number <10, indicating 3% remaining acid [65]. Once completed, 100 ppm of hydroquinone (0.02 g) was added to the resin to prevent any premature polymerization.

This procedure was repeated for tert-butyl phenol in place of phenol to form BPMEM828, NC-510 in place of phenol to form NC510MEM828, and NX-2026 in place of phenol to form NX2026MEM828. This procedure was also repeated to form IPNs with varying HELOXY™ Modifier 68 (HM68) ratios of approximately 10 and 25 wt% to Epon828.

Figure 3

Reaction Scheme of PMEM828 Synthesis

Step 1:

phenol + methacrylic anhydride → (DMAP, 50-55 ºC, Argon, Solventless) → phenyl methacrylate + methacrylic acid

Step 2:

methacrylic acid + Diglycidyl Ether of Bisphenol A (Epon828) → (AMC-2, 70 ºC, Air, Solventless) →

Partially Methacrylated Diglycidyl Ether of Bisphenol A (EM828)

25
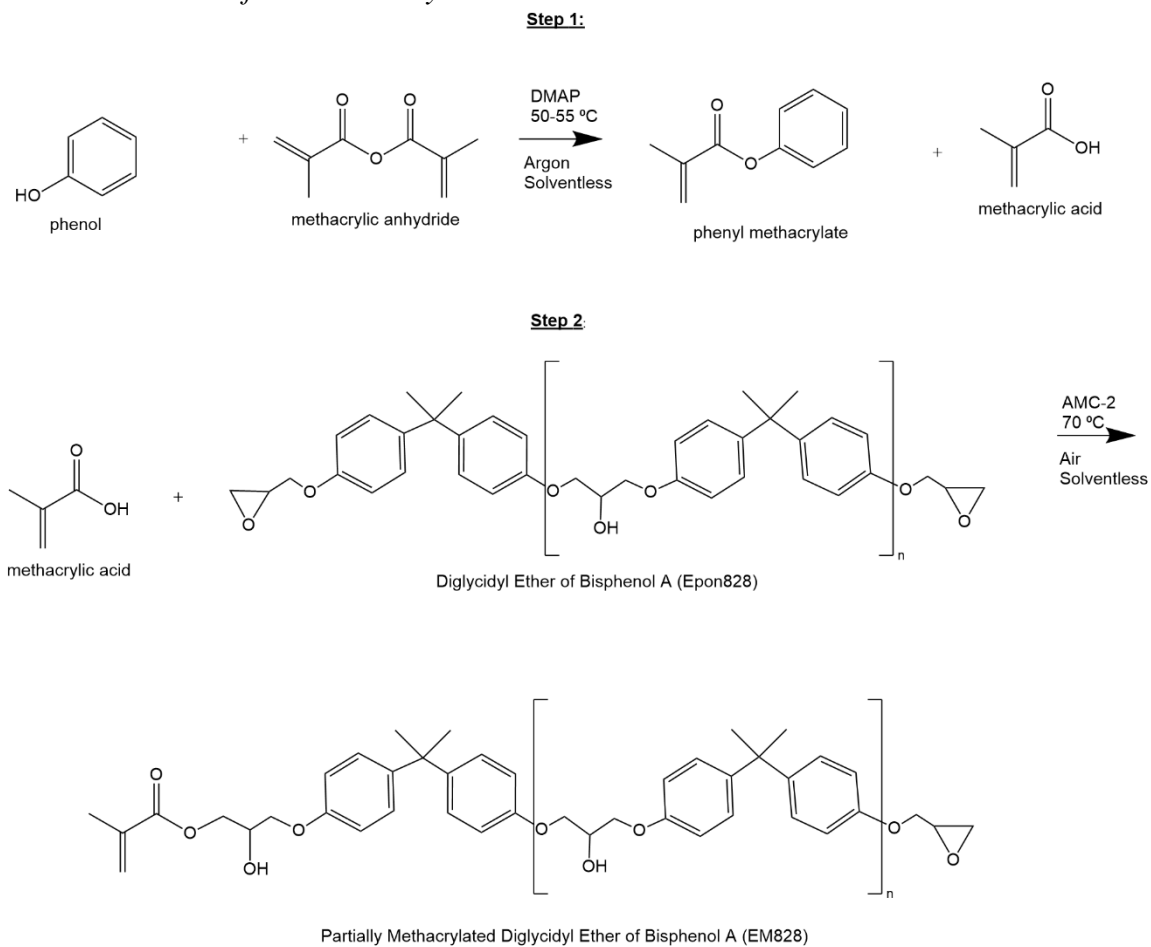
3.4 Resin Rheology

Viscosities for each synthesized resin were collected using a TA Instruments Discovery Hybrid Rheometer (DHR-2) using a 1° 40 mm cone geometry at a temperature of 25°C. All measurements were taken using a shear rate that was ramped logarithmically increasing from 1 to 100 s^{-1} and decreasing from 100 to 1 s^{-1} [16], [67], [68].

3.5 Resin Formulation

Each resin was formulated with TPO, at 2 wt% of the total mass of the reaction, to facilitate the free radical polymerization between the methacrylate functionalities. Epikure W was added to initiate the cure of the epoxy-amine network with the assumption that the conversion to the dual functional monomer EM828 was 100% [34]. The amount of Epikure W added to each formulation was determined via the theoretical epoxy equivalent weight (EEW) of each resin system. The EEW found by calculating the molecular weight of the polymer per active site, which in the case of the epoxy-amine network was the epoxy functional group. A stoichiometric amount of Epikure W was added to the resin in correspondence to the procedure found in Hernandez et al. [69], [70]. Once the curing agent and photoinitiator were added to the resin, all components were mixed using a Thinky ARE-310 planetary mixer for 10 minutes at 2000 rpm and subsequently defoamed for 5 minutes at 2200 rpm. The mixing cycle was performed twice to ensure full dissolution of photoinitiator and curing agent.

3.6 Resin Additive Manufacturing & Cure

After formulation, each resin was prepared for free radical photopolymerization
via a Formlabs Form 2 SLA Printer. All prints were conducted using a selected layer
height of 100 µm, with the preprogrammed parameters associated with the chosen setting
"Tough V5" in "Open Mode", to maintain consistent processing parameters with Bassett
et al. [34]. Digital models were made in preparation for viscoelastic, compression, and
fracture testing and uploaded to the Form 2 using Formlabs printing software PreForm as
shown in Figure 5. After printing, all samples were washed in a Formlabs Form Wash
using IPA for 20 minutes to remove any uncured residue from the green polymer. These
samples were denoted as AM samples. Once washed, the samples were subsequently
post-processed using Formlabs Form Cure (labeled FC), which heats the samples to 80$^{\text{o}}$
C for 2 hours under UV/visible light (λ= 405 nm). After the FC step, the samples are
further post-cured at 180$^{\text{o}}$ C in a thermal oven for 2 hours (denoted PC).

Figure 4

Arrangements of Printed DMA Bars, Fracture Bars, and Compression Cylinders with Supports on Build Platform via Formlabs Preform
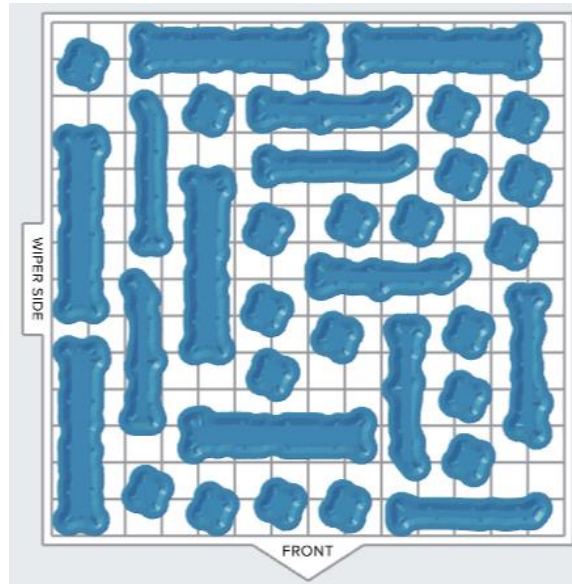
3.7 Extent of Cure

Extent of cure values for all printed polymers were obtained at each various stage of the curing process using near-IR spectroscopy. An IR spectrum using a Thermo Scientific Nicolet iS50 FTIR equipped with a CaF_2 beam splitter was taken of the formulated resin using a glass well with a path length of 3 mm. The subsequent curing steps which included the green polymer after print (AM), the polymer after Form Cure (FC), and thermal post-cure (PC) were all measured with IR at a thickness of 2.5 mm. All IR spectrums were taken with 64 scans at a resolution of 2 cm^{-1} to quantify the

conversion of the methacrylate, epoxies, and primary amines at various stages of processing.

To calculate the extent of cure for both the methacrylate modalities and epoxy-amine modalities, 3 peaks were assessed at each state of cure with near-IR. All peaks were normalized against a reference peak at 5900 cm^{-1} corresponding to the carbon chain backbone of the polymer network that does not participate in polymerization [71]. The peak measured at 6165 cm^{-1} was used to quantify the extent of cure for the methacrylate network of the IPN as shown in Equation 8. For quantitative analysis changes in both epoxy and primary amines can be directly determined through near-IR to illustrate the formation of the epoxy-amine network [72].The degree of conversion for the epoxy-amine network was assessed using the integration at band 4530 cm^{-1} to designate the oxirane functional group as shown in Equation 9. The primary amine which is visible at 5000 cm^{-1} was used for the qualitative assessment of the formation of the epoxy-amine network as shown in Equation 10. A representative FT-IR spectrum of PMEM828 at each stage of cure is shown in Figure 6.

$$X(methacrylate) = \frac{\left(\frac{A_{6165\ cm^{-1}}}{A_{5900\ cm^{-1}}}\right)_{resin} - \left(\frac{A_{6165\ cm^{-1}}}{A_{5900\ cm^{-1}}}\right)_{polymer}}{\left(\frac{A_{6165\ cm^{-1}}}{A_{5900\ cm^{-1}}}\right)_{polymer}} \qquad (8)$$

$$X(oxirane) = \frac{\left(\dfrac{A_{4530\ cm^{-1}}}{A_{5900\ cm^{-1}}}\right)_{resin} - \left(\dfrac{A_{4530\ cm^{-1}}}{A_{5900\ cm^{-1}}}\right)_{polymer}}{\left(\dfrac{A_{4530\ cm^{-1}}}{A_{5900\ cm^{-1}}}\right)_{polymer}} \qquad (9)$$

$$X(amine) = \frac{\left(\dfrac{A_{5000\ cm^{-1}}}{A_{5900\ cm^{-1}}}\right)_{resin} - \left(\dfrac{A_{5000\ cm^{-1}}}{A_{5900\ cm^{-1}}}\right)_{polymer}}{\left(\dfrac{A_{5000\ cm^{-1}}}{A_{5900\ cm^{-1}}}\right)_{polymer}} \qquad (10)$$

Figure 5

Near-IR Spectra for PMEM828 at Various Stages of Cure
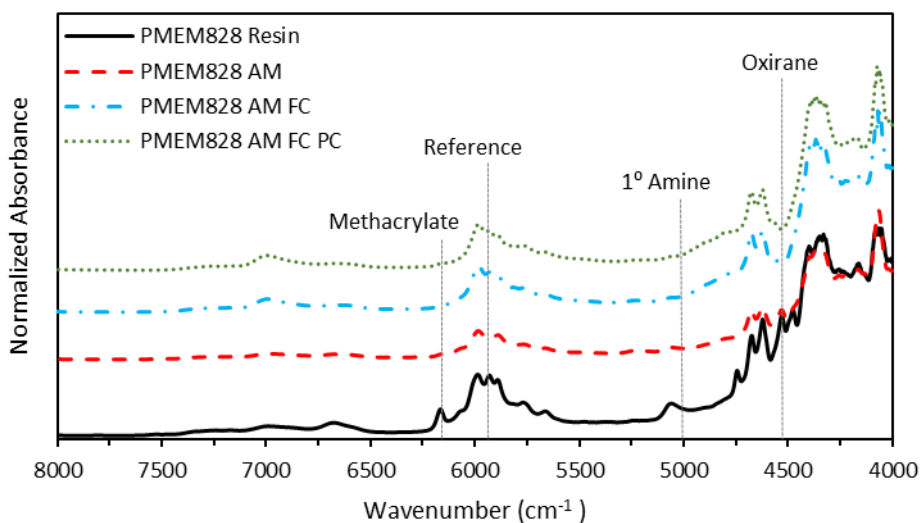
Note. Spectra are offset vertically for clarity.

The extent of cure is typically measured via DSC as a ratio between heat released by the reaction and the total heat released. While this procedure is useful, it lacks the accuracy at high degrees of cure and faster reactions [72]. In this work, DSC was used in tandem with FTIR to verify the extent of reaction for each polymer network formed. All samples were measured using a TA Instruments Discovery DSC 2500 to confirm that each system was fully cured after the subsequent processing steps. A Tzero aluminum pan was loaded with 5-10 mg of sample and sealed with a Tzero lid. Two heating and cooling cycles were performed at a rate of 10 $^{\circ}$C per minute under inert conditions (N_2) from 0 – 250 $^{\circ}$C. The second cycle was evaluated for any appreciable exotherms to indicate further curing of polymer. This procedure was performed in duplicate for each processed polymer.

3.8 Polymer Properties

All samples were evaluated for thermal properties using a TA Instruments Discovery Thermogravimetric Analyzer 550 (TGA) under both inert (N_2) and oxidative (air) environments (40 mL min^{-1} balance gas flow rate and 25 mL min^{-1} sample gas flow rate). Approximately 10 mg of sample were loaded into a platinum pan and heated to 700 $^{\circ}$C at a ramp of 10°C per minute. Initial decomposition temperature (IDT), temperature at 50 wt% degradation ($T_{50\%}$), temperature at maximum degradation (T_{max}) and char content are reported for each sample. This procedure was performed in duplicate for each processed polymer under each environment.

A TA Instruments Q800 Dynamic Mechanical Analyzer was used to assess all viscoelastic properties of the fully cured formulations. All samples were prepared using the appropriate dimensions ($35 \times 12 \times 2.5$ mm^3 and $35 \times 12 \times 1.5$ mm^3) chosen in accordance to McAninch et al [73]. All samples were affixed with a single cantilever geometry using a torque wrench with 7.5 in-lbs of force. Tests were conducted at a frequency of 1.0 Hz, an oscillation amplitude of 7.5 µm, and a Poisson's ratio of 0.35 over a temperature sweep from 0 to 250 ^{o}C with a rate of 2 ^{o}C per minute. For this work, the peak of the loss modulus (E'') and the peak of the tan δ curves were reported to represent values for the T_g of each material. The glass storage modulus (E') was reported at 25 ^{o}C and the effective molecular weight between crosslinks (M_c) was calculated according to the Theory of Rubbery Elasticity [74]. Density (ρ) of each sample was determined at 25 ^{o}C via Archimedes' principal [75]. Viscoelastic data for each cured resin was collected in triplicate for both thin (1.5 mm) and thick (2.5 mm) specimens.

All mechanical properties were determined using an Instron 5966 mechanical testing instrument. For compression testing, cylindrical samples were prepared with a diameter of 6.4 mm and a length of 12.7 mm. Each specimen was tested using a 10 kN load cell at a crosshead speed of 1.3 mm per minute and analyzed in accordance to ASTM D695-15 [60]. The maximum compressive strength as well as compressive modulus at 2% strain, were determined for each cured resin system with a minimum of 5 samples. For fracture toughness, samples were prepared and analyzed according to ASTM D5045-14 [62]. Samples were printed with the dimensions $44 \times 10 \times 4$ mm^3 and fully cured before being notched with a diamond saw. Once notched, each sample was

scored using a freshly opened razor blade to propagate a crack [63]. Samples were then assessed using the Instron 5966 affixed with a 1 kN load cell and 3-point bend flexure fixture at a cross head speed of 10 mm per minute until failure. Upon fracture failure, the plane-strain fracture toughness, K_{IC}, and the critical strain energy release rate, G_{IC}, were determined for each cured system with a minimum of 5 replicates.

Chapter 4

Results and Discussion

4.1 Effects of Removing AMC-2 Catalyst

4.1.1 Introduction

The synthesis of PMEM828 (EEW = 621 g mol^{-1}) was completed in a 1P2S

mechanism as depicted in Chapter 3. The first step, where the esterification of phenol

with methacrylic anhydride to produce phenyl methacrylate and methacrylic acid, is

catalyzed by tertiary amine DMAP. The second step, where the Epon828 is partially

methacrylated by methacrylic acid, is typically catalyzed by chromium-based catalyst

AMC-2. AMC-2 was once produced by AMPAC fine chemicals but has since been

discontinued as a result of the continuing effort to remove or limit the use of Cr(VI) from

manufacturers [76]. As a result, there has been increased motivation to find an alternate

catalyst for the second step of the 1P2S mechanism. Werner J. Blank has investigated the

epoxy-carboxyl reaction, like the one in step 2 of the 1P2S, and found a wide range of

amines, phosphonium and metal catalysts that have successfully facilitated the reaction

[77]. In Blank's studies, the overall effectiveness of each catalyst was observed in

addition to the deficiencies associated with each catalyst in the production of epoxy-

based coatings. Some of the notable shortcomings in Blank's work were the tendency of

different catalysts to yellow and the reduction in the stability of the coatings studied [77].

Upon further investigation, we hypothesized that the tertiary amine (DMAP)

used in the first step of synthesis could potentially catalyze the epoxy-carboxyl reaction

in the second step as well. To evaluate the effectiveness of DMAP in the second step, the polymer properties of PMEM828 catalyzed with and without AMC-2 in the second step were closely compared. To address concerns related to the stability of the resin, rheology measurements and ^{1}H-NMR spectra were collected each week for the span of 4 weeks to monitor any changes in resin viscosity or chemical structure.

4.1.2 Resin Stability

Two batches of PMEM828 were prepared side by side using the same 1P2S methodology as explained by Bassett et al [34]. One batch was prepared with AMC-2 catalyst in step 2 and the second batch was prepared with no catalyst in step 2 with the intent of the DMAP present in step 1 catalyzing the epoxy-carboxyl reaction between Epon828 and methacrylic acid. The resin stability of this reaction was monitored via changes in viscosity at both ambient and chilled conditions as well as ^{1}H-NMR analysis.

Both resins displayed Newtonian behavior despite the presence of AMC-2 catalyst. Changes in resin viscosity as a function of time are displayed in Figure 7. Values for all resin viscosities stored at different conditions are listed in Table 1.

Figure 6

Viscosities of Both PMEM828 Catalyzed With and Without AMC-2 Plotted as a Function

of Time
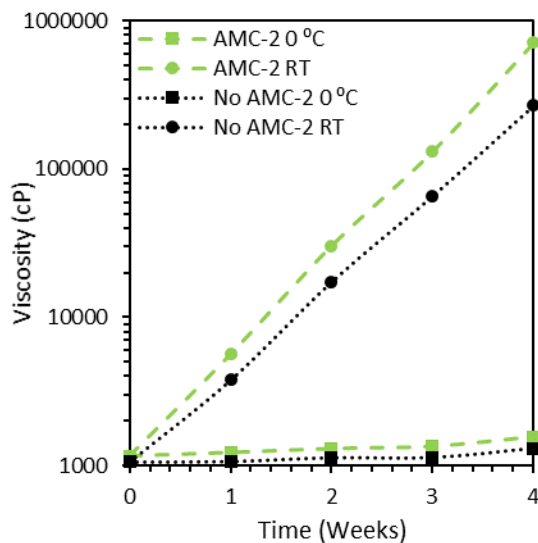
Note. Lines do not depict trend but added for benefit of reader. Please refer to table for standard deviation.

Table 1

Resin Viscosities of PMEM828 Catalyzed With and Without AMC-2 Over 4 Weeks

	Viscosity at 25°C (cP)			
	No AMC-2 RT	*AMC-2 RT*	*No AMC-2 0°C*	*AMC-2 0°C*
Week 0	1058 ± 25	1162 ± 18	1058 ± 25	1162 ± 18
Week 1	3769 ± 129	5640 ± 25	1067 ± 14	1225 ± 26
Week 2	17360 ± 300	30400 ± 670	1131 ± 18	1301 ± 21
Week 3	66000 ± 2400	132000 ± 5900	1135 ± 59	1347 ± 52
Week 4	268000 ± 12000	714000 ± 25000	1306 ± 50	1559 ± 58

Both resins stored at 0 °C, in a refrigerator, showed minimal increase in resin viscosity. PMEM828 with AMC-2 catalyst in the 2nd step increased in viscosity from 1162 cP to 1559 cP. Despite this 35% increase in viscosity, at 1500 cP this resin is still appropriate for SLA applications. PMEM828 without AMC-2 in step 2 increased in viscosity from 1058 cP to 1306 cP. The absence of AMC-2 resulted in a lower viscosity resin that only increased by 23% compared to the 35% growth exhibited by the chromium containing resin. This difference will not impact the intended use of the resin and shows that the resin still behaves similarly under chilled conditions without AMC-2 present. This is further supported by the behavior of both resins at room temperature.

At ambient conditions, PMEM828 with AMC-2 catalyst increased from 1162 cP to 714,000 cP after 4 weeks. By removing the AMC-2 catalyst in the second step the viscosity of PMEM828 at room temperature grew from 1058 cP to 268,000 cP which is close to 1/3 of the growth displayed in PMEM828 with AMC-2 catalyst. Despite the difference in viscosity at the end of the 4-week study, both resins showed tremendous increases in viscosity as soon as week 1. At week 1, both resins that were stored under ambient conditions would be poor candidates for SLA. Resins used for SLA are typically preferred to be 500-1500 cP at 25 °C but can sometimes be used at ambient conditions if they are up to 3000 cP [10], [65]. This shows, from a viscosity perspective, there is no risk removing AMC-2 catalyst from the second step of the 1P2S synthesis.

Further stability studies were conducted using ^{1}H-NMR analysis. Each week, both chilled and ambient samples of PMEM828, with and without AMC-2 catalyst, were analyzed via ^{1}H-NMR to assess any changes in chemical structure over 4 weeks.

Representative ^{1}H-NMR spectra are shown for PMEM828 catalyzed both with and without AMC-2 at the beginning of the study, in Figure 8 and Figure 9, respectively.

Figure 7

^{1}H-NMR Spectra of PMEM828 Catalyzed With AMC-2 at Week 0
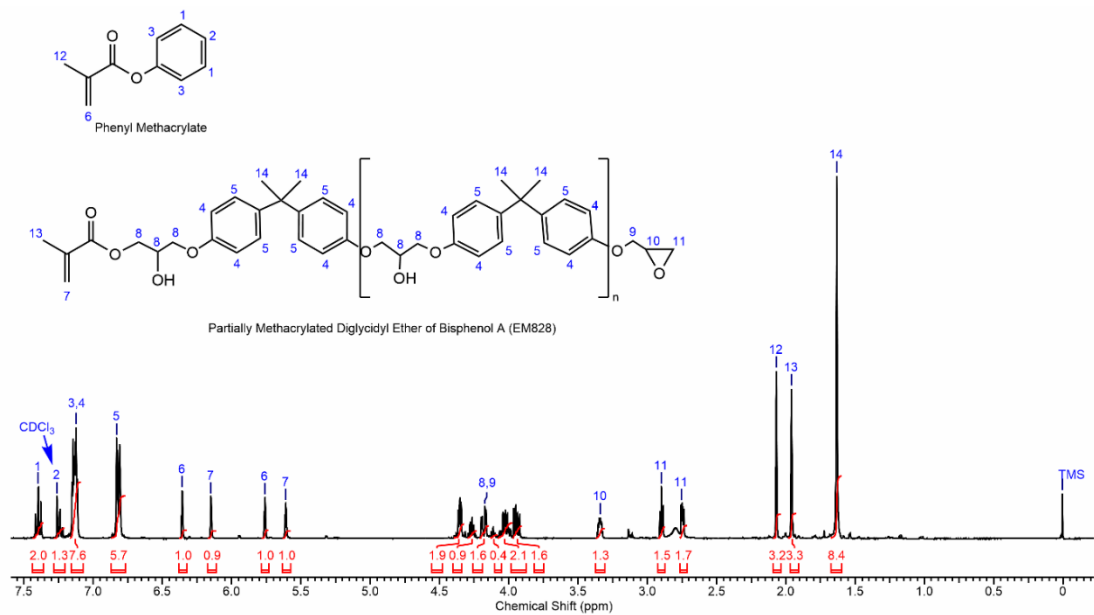
Figure 8

¹H-NMR Spectra of PMEM828 Catalyzed Without AMC-2 at Week 0
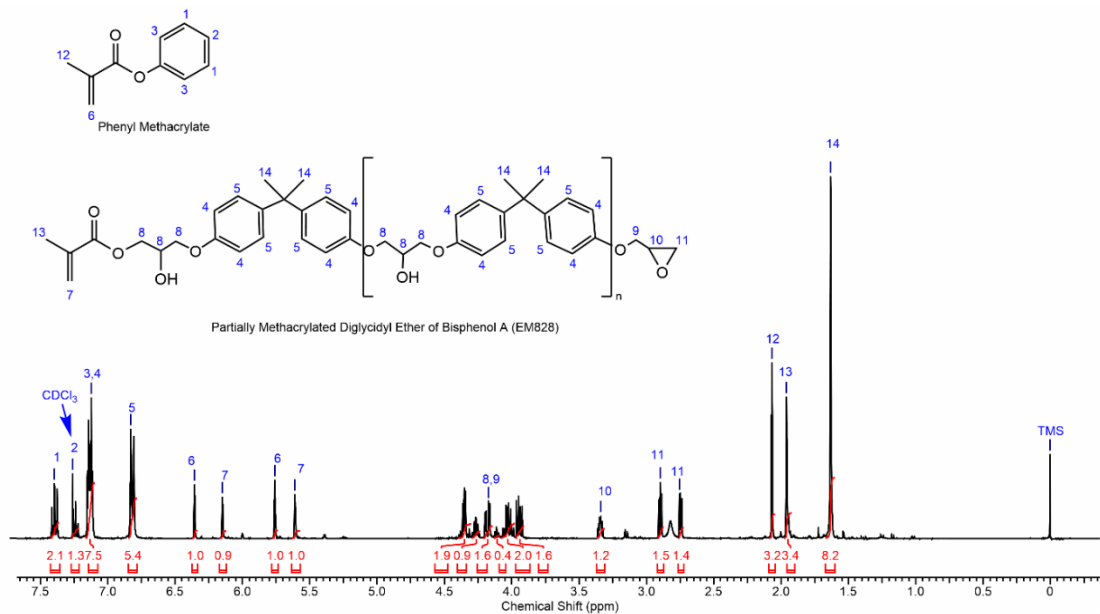
Both ¹H-NMR spectra reveal the removal of AMC-2 catalyst did not impact the formation of either phenyl methacrylate or EM828. Deviations of peak integrations between PMEM828 catalyzed with and without AMC-2 catalyst can be attributed to differences in kinetics of reaction, which is beyond the scope of this work.

The primary areas of interest of the ¹H-NMR study were focused on the protons associated with the epoxy on EM828 at chemical shifts 2.76, 2.9, and 3.34 ppm as well as the protons from ~4-4.5 ppm. At the beginning of the study, protons from 4-4.5 ppm would correspond to hydrogens of the hydroxy propyl ether linkages. However, as time progresses the number of protons between 4-4.5 ppm is expected to increase in the ¹H-NMR as an indication of epoxy homopolymerization while the number of protons from

39

the epoxy will decrease. Anionic epoxy homopolymerization can be initiated by tertiary

amines such as DMAP, as well as imidazoles and ammonium salts [78]. Typically, these

polymerizations with tertiary amines are distinguished by complex reaction mechanisms

and slow reaction rates. For the intent of manufacturing IPNs via sequential curing,

premature homopolymerization of the epoxy would greatly affect the formation of the

polymer structure and are therefore undesired. Representative ^{1}H-NMR spectra from

weeks 0, 2 and 4 of PMEM828 catalyzed without AMC-2 are illustrated in Figure 10

with the highlighted regions of interest to quantify epoxy homopolymerization.

Figure 9

Stacked ^{1}H-NMR Spectra of PMEM828 Over 4-Week Stability Study
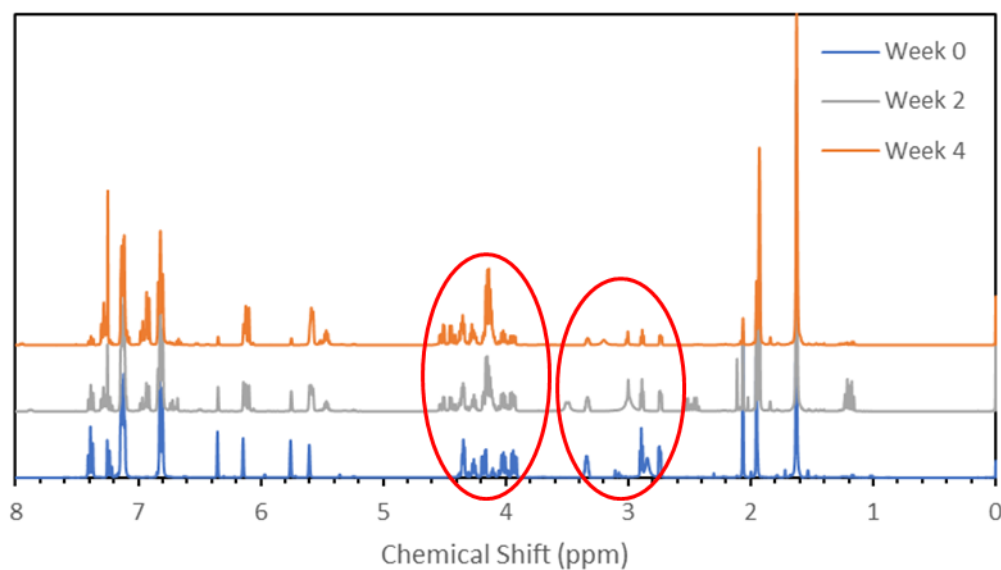
Note. Circles are highlighting regions of interest.

As predicted, the number of protons between 4.0-4.5 ppm increased while the number of protons belonging to the epoxy modality decreased. Changes in other regions were observed but they were not indicative of epoxy homopolymerization. Significant changes to the methyl group on phenyl methacrylate, the carbonyl group on phenyl methacrylate, and the aromatic region of both phenyl methacrylate and EM828 were observed over the 4-week investigation. Changes in these regions suggest other changes occurring between the methacrylate functionality on phenyl methacrylate as well the aromatic character of both phenyl methacrylate and EM828. These phenomena cannot easily be explained but could perhaps be a caveat to the complicated reaction mechanism for the anionic polymerization of epoxy monomers initiated by tertiary amines [78], [79]. However, more work would need to be done in the future to further investigate these phenomena.

To effectively quantify the degree of homopolymerization occurring during the stability study, the % conversion of epoxy was tracked each week and displayed in Figure 11. In addition to the conversion of epoxy, the number of protons corresponding to the range indicative of epoxy homopolymerization were also tracked and shown in Figure 12. Additional ^{1}H-NMR spectra from the 4-week stability study can be found in Appendix A.

Figure 10

Conversion of Epoxy Determined via ^{1}H-NMR During 4-Week Stability Study
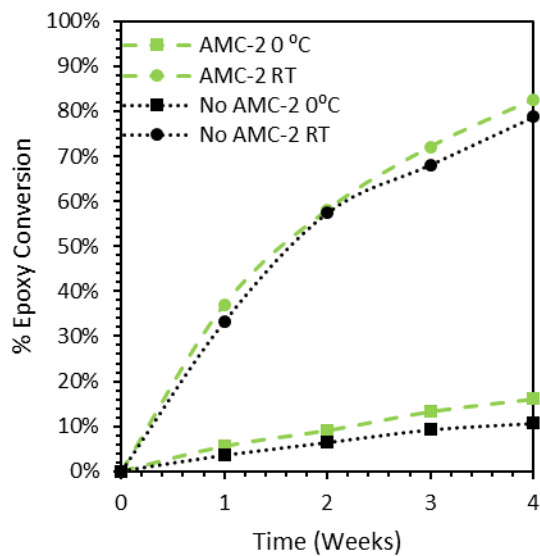
Note. Lines do not depict trend but added for benefit of reader.

Figure 11

Protons Corresponding to Epoxy Homopolymerization via ^{1}H-NMR During 4-Week
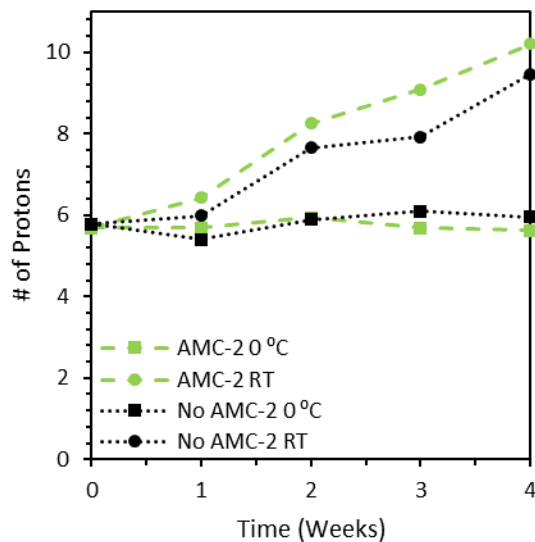
Stability Study

Note. Lines do not depict trend but added for benefit of reader.

Over the course of the 4-week stability study there was a small degree of epoxy
conversion for resins kept at 0$^\text{o}$C of approximately 10-15%. Under refrigerated conditions
both resins exhibited a much lower extent of conversion for epoxies then the respective
resins kept at ambient conditions. Under ambient conditions, PMEM828 catalyzed both
with and without AMC-2 yielded an epoxy conversion of around 80%, indicating a high
degree of epoxy homopolymerization. These findings were further supported by the
increasing number of protons between chemical shifts 4.0-4.5 ppm. At ambient
conditions, the number of protons for both PMEM828 resins catalyzed with and without

AMC-2 were found to increase from about 6 protons to almost 10 by the end of the 4-week study. For resins kept at 0 °C, ^{1}H-NMR revealed little deviation for the number of protons in that region over 4-weeks, suggesting little to no homopolymerization of the epoxies. While little deviation was shown, these discrepancies can be attributed to the resonance of hydrogen bonding from the hydroxyl group on EM828. Due to the variable extent of hydrogen bonding, the position of hydroxyl resonances will vary greatly and at times can overlap with peaks corresponding to the epoxy protons [45].

Observing changes in viscosity and chemical composition of PMEM828 resin catalyzed both with and without AMC-2 in the second step showed little risk in removing the chromium catalyst from the 1P2S synthesis. When kept at ambient conditions, PMEM828 will gel at room temperature and exhibit a high degree of epoxy homopolymerization due to the DMAP used in step 1. The stability of PMEM828 at ambient conditions will not change regardless of what catalyst is used in the second step of the 1P2S synthesis. At 0 °C, or under chilled conditions, there is little observed fluctuation in resin viscosity and no quantifiable degree of epoxy homopolymerization for both versions of PMEM828. The lack of change in resin stability with the removal of the chromium-based catalyst suggests proceeding to synthesize PMEM828, as well as similar resin systems, without AMC-2 a viable option moving forward.

4.1.3 Polymer Properties

Removing the AMC-2 catalyst from step 2 resulted in a clear neat resin before the addition of curing agent and photointiator. Once cured, both polymers with and without AMC-2 were dark brown due to the Epikure W and slight oxidation from post-processing

steps. Processed polymers manufactured during this study were also hard and glassy.

TGA was conducted under inert conditions of each fully cured IPN and representative

thermograms are displayed in Figure 13. The values of IDT, T_{50}, T_{max}, and char content

were collected and reported in Table 2. Thermograms run under an oxidative atmosphere

and the measured thermogravimetric values can be found in Appendix B.

Figure 12

TGA Thermograms and Respective 1st Derivative of PMEM828 Catalyzed With and
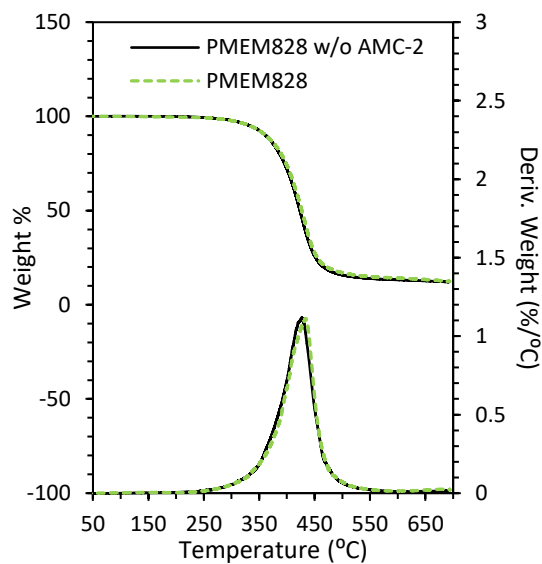
Without AMC-2 in N$_2$

Table 2

Thermogravimetric Analysis Data of PMEM828 Catalyzed With and Without AMC-2 in

N_2

Sample	IDT (°C)	$T_{50\%}$ (°C)	T_{max} (°C)	Char Content (%)
PMEM828	335 ± 1	428 ± 1	433 ± 1	12.76 ± 0.32
PMEM828 w/o AMC-2	337 ± 3	424 ± 1	426	11.27 ± 0.81

Thermogravimetric analysis revealed no significant changes in thermal degradation properties with the removal of AMC-2 catalyst in the second step of 1P2S synthesis. In the case of eliminating AMC-2 catalyst based on thermal decomposition rates, the results are statistically insignificant from one another. This is further supported with a $T_{50\%}$ of approximately 425 °C, a T_{max} between 426-433 °C, and a char content of roughly 12%. Similar trends were observed under oxidative conditions except for the char content which is due to the char left over being completely combusted at higher temperatures [80].

The viscoelastic properties of PMEM828 with and without AMC-2 catalyst, were measured with DMA. Thermograms in Figure 14 display representative storage moduli (E') and loss moduli (E'') while Figure 15 exhibits representative tan δ curves for both IPNs. All measured and calculated values found with DMA are reported in Table 3. Additional DMA data can be found in Appendix C.

Figure 13

DMA Thermograms of E' and E'' For all PMEM828 With and Without AMC-2
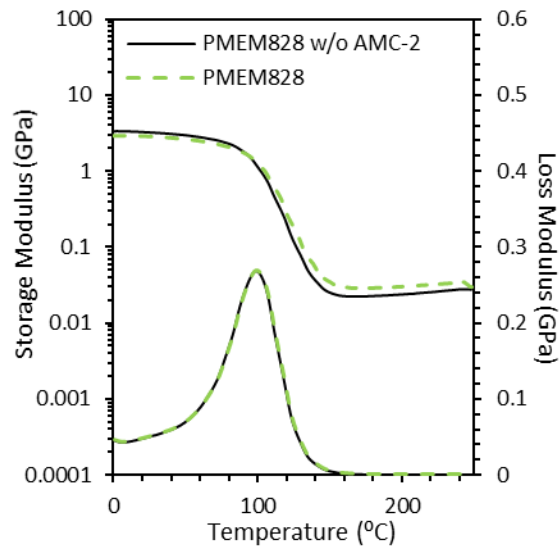
Figure 14

DMA Thermograms of Tan δ for All PMEM828 With and Without AMC-2
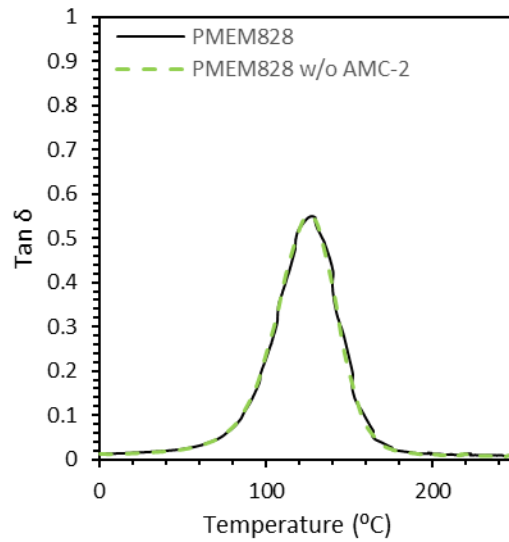
Table 3

Viscoelastic Data of PMEM828 With and Without AMC-2

Sample	E′ @ 25 °C (GPa)	Peak of E″ (°C)	Peak of Tan δ (°C)	M_c (g mol^{-1})	ρ @ 25 °C (g cm^{-3})
PMEM828	3.1 ± 0.2	98 ± 2	129 ± 2	446 ± 14	1.198 ± 0.001
PMEM828 w/o AMC-2	3.0 ± 0.2	102 ± 1	133 ± 1	569 ± 12	1.199 ± 0.001

Analysis of thermomechanical properties reveal no significant difference between the catalyst used in step 2 of the 1P2S synthesis of PMEM828. At 25 °C both IPN exhibit the same level of stiffness with a E' of around 3.1 GPa which are similar to E' of conventional styrene-diluted vinyl ester resins (VERs) [68]. The shape and curve of the loss modulus show that the networks form in close enough orientations that the same amount of energy is dissipated throughout the structure. With a conservative T_g of nearly 100 °C signified by the peak of E'' and the peak of tan δ around 130 °C, the AMC-2 does not contribute to the temperature at which the amorphous polymer changes from a glassy to rubbery state. Both prepared IPN systems exhibited comparable T_g values to conventional styrene-diluted (VERs) [68]. The shapes of both tan δ further support the lack of difference between structures with the same size and shape [58]. Since PMEM828 has similar chain orientation and behavior with and without AMC-2, we can assume that the same degree of crosslinking can be observed in both formulations. An M_c of 446 g mol^{-1} was calculated for PMEM828 with AMC-2, while an M_c of 569 g mol^{-1} suggested a lower degree of crosslinking when AMC-2 was removed. While these two values are statistically different from one another they are both well within error when compared to

an M_c of 511 ± 104 g mol^{-1} originally reported by Bassett et al [34]. Similarities in properties determined via DMA, illustrate the way the structure of PMEM828 is formed and may indicate similarities in mechanical performance.

Mechanical properties for PMEM828 synthesized both with and without AMC-2 catalyst in the second step were quantified through compressive strength and fracture toughness. Representative stress-strain curves from compression testing for both formulations are displayed in Figure 16. The maximum strength reached at compressive failure and compressive modulus were evaluated and listed in Table 4.

Figure 15

Stress-Strain Curves of PMEM828 With and Without AMC-2
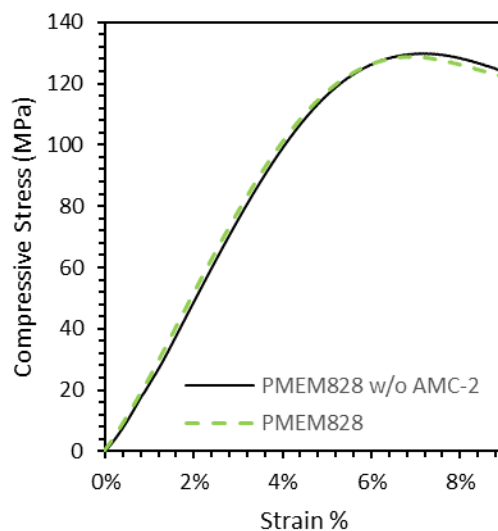
Table 4

Compression Testing Values PMEM828 With and Without AMC-2

Sample	Compressive Strength (MPa)	Compressive Modulus (MPa)
PMEM828	129 ± 7	2346 ± 273
PMEM828 w/o AMC-2	131 ± 3	2409 ± 181

Compression testing reveals that the compressive strength of PMEM828 remained around 130 MPa with the removal of the AMC-2 catalyst. This trend is supported by the statistically insignificant difference between compressive moduli of the two tested formulations which both averaged around 2,400 MPa. Results indicate that when exposed to compressive mechanical stress, PMEM828 will behave the same regardless of the presence of AMC-2 catalyst in the second step.

Further structural analysis was performed through fracture toughness experiments. Representative load-displacement curves are presented in Figure 17. Critical strain energy release rate, G_{1C}, and plane-strain fracture toughness, K_{1C}, were also evaluated for PMEM828 catalyzed both with and without AMC-2 and listed in Table 5.

Figure 16

Load-Displacement Curves for PMEM828 With and Without AMC-2
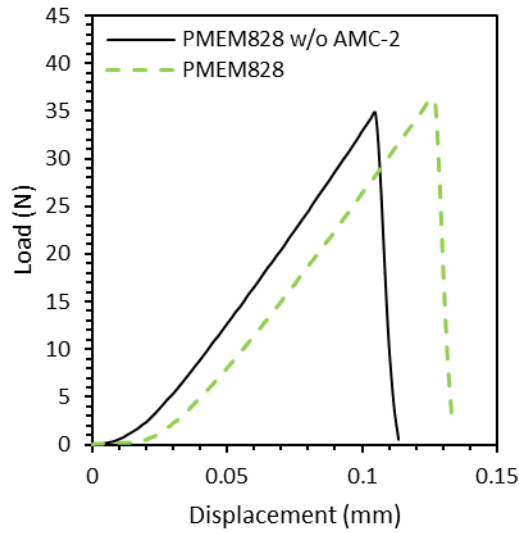
Table 5

Fracture Toughness K_{1C} and G_{1C} Values For PMEM828 With and Without AMC-2

Sample	G_{1C} (J/m²)	K_{1C} (MPa m$^{1/2}$)
PMEM828	140 ± 14	0.63 ± 0.09
PMEM828 w/o AMC-2	169 ± 61	0.75 ± 0.15

The removal of the AMC-2 catalyst in the second step slightly raised the G_{1C}

and K_{1C} from 140 J/m² to 169 J/m² and 0.63 MPa m$^{1/2}$ to 0.75 MPa m$^{1/2,}$ respectively.

Both data sets were determined to be the same statistically via a *t*-test and were in

agreement with reported G_{1C} values of Epon828-Epikure W resin systems of 135 J m^{-2}

[81]. This final mechanical test proved that AMC-2 catalyst was not necessary in the second step of the 1P2S synthesis to provide PMEM828 the same polymer structure and mechanical performance. Despite the difference in selectivity between AMC-2 catalyst and tertiary amines, the fracture toughness does not suggest a dependence on AMC-2 and will not suffer in the absence of the chromium catalyst.

4.2 Modifying Step 1 of 1P2S

4.2.1 Introduction

The main goal of this section is to explore how altering the first step in the 1P2S synthesis scheme affects the thermal and mechanical performance of the IPN. Different industrial markets, regional regulations, and product application methods dictate the level of scrutiny that certain compounds are viewed considering their presence at residual levels in final products. For these reasons, phenol was replaced with the phenol derivatives shown in Figure 18, to be viewed more favorably when present in chemical products at trace residual concentrations. By performing these substitutions, the resulting resins and polymers formulated were examined for changes in resin viscosity, extents of cure, thermogravimetric properties, viscoelastic properties, and mechanical performance.

Figure 17

Chemical Structures of Phenol Derivatives Used in Step 1 of 1P2S Synthesis

Cardolite NX-2026

4-(*tert*-butyl)phenol

Cardolite NC-510
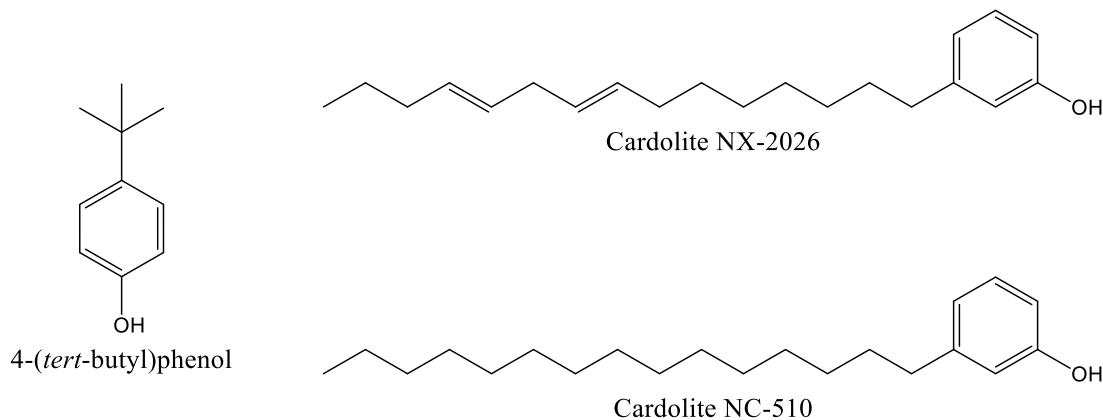
4.2.2 Cardanol Formulations

Cardanol is a phenolic lipid that is derived from a byproduct of the cashew industry and has gained serious interest over the years as a means to creating biobased polymers and additives [82]. A liquid referred to as cashew nutshell liquid (CNSL) lies within the shell of a cashew nut and can be extracted and refined to make cardanol [83]. The area of interest particular to cardanol is the unsaturated aliphatic chain in the meta position with respect to the hydroxyl group which is known to impart flexibility, good chemical resistance, wettability, and compatibility in various resins, films, and coatings. As a phenolic derivative, there are many different ways cardanol can be modified to produce cardanol based phenolic resins, epoxy resins, cardanol based acrylates, and vinyl ester resins [84].

53

In this study, cardanol with an unsaturated aliphatic chain (NC-510) and cardanol with 2 double bonds along the aliphatic chain (NX-2026) were chosen as potential alternatives to phenol in the 1P2S synthesis of PMEM828 to create NC510MEM828 and NX2026EM828, respectively. Cardanol based monomers with methacrylate functionality have been prepared through different methodologies than the esterification presented in the 1st step of the 1P2S synthesis of PMEM828 [85], [86], [87]. However, it was assumed that replacing cardanol with a 1:1 mole ratio with phenol in the 1st step of the 1P2S mechanism would successfully produce cardanol methacrylate and methacrylic acid without changing any of the reaction parameters.

Neither NC510 and NX2026 could be fully methacrylated in the 1st step of the 1P2S synthesis of NC510MEM828 and NX2026MEM828. In the past, the Centre for Polymer Science & Engineering have been able to synthesize cardanol methacrylate by adding methacryloyl acid to a solution of cardanol, tertiary amine, and inhibitor at low temperatures. The solution was then heated to 50 ⁰C for 1 hour before cooling to room temperature overnight and being washed with benzene, hydrochloric acid and ice water [86]. Differences between this methodology and the 1P2S mechanism proposed in our lab, lie between the choice of chemicals used to facilitate the reaction and the various washing steps required to isolate the product. The 1P2S synthesis removes the need for product isolation before use which results in less chemicals and steps required. The need to wash the reaction at the end suggest a large amount of byproducts produced from the high amount of catalyst used and the increased reactivity of methacryloyl chloride compared to methacrylic anhydride [41]. Using such large amounts of tertiary amine,

54

reactive materials such as methacryloyl chloride, and hazardous chemicals like benzene, have proved this method to be outdated and dangerous. Recently, methacrylated cardanol has been synthesized in a 1P2S methodology by Li et al. by forming hydroxyethylated cardanol with ethylene carbonate and high purity cardanol in the first step and then producing cardanol methacrylate in the second step [87]. After the first step, hydroxyethylated cardanol was added to dry dichloromethane and triethylamine in a round bottom flask. Once combined, the solution was purged with nitrogen and immersed into an ice bath while methacrylic anhydride was added and allowed to react for 18 hours. This 1P2S synthesis still required the need for washing with various solvents and drying to isolate the final product.

While it is possible to synthesize cardanol methacrylate to high levels of purity with methacrylic anhydride, the reaction parameters need to be optimized in the 1P2S mechanism proposed by our lab. Optimization of parameters for an esterification reaction of cardanol could be dependent on the effect of catalyst loading, the effect of temperature, and the effect of molar ratio of reactants [88]. While reaction parameters can be optimized to achieve the first step of the mechanism of the reaction schema, the second step may not successfully partially methacrylate epon828 and fail to form the desired IPN. Due to the incompatibility between cardanol and our 1P2S synthesis of SLA resin, the only alternative phenolic used in this study was 4-tertbutylphenol to make BPMEM828.

4.2.3 Resin Rheology

Both PMEM828 and BPMEM828 resin displayed Newtonian behavior. The viscosity of each resin was evaluated based on the average of three steady state points along different shear rates and are shown in Table 6. Typically, lower viscosity resins are desired for SLA applications to ensure good back fill of the resin between the formation of each layer. The preferred resin viscosity for SLA are generally between 500-1500 cP at room temperature, but resins with viscosities as high as 3000 cP have also been successful in rapid prototyping techniques [10], [65].

Table 6

Viscosities of PMEM828 and BPMEM828 Resins at 25 ⁰C

Sample	Viscosity at 25 ^{o}C (cP)
PMEM828	1082 ± 30
BPMEM828	2442 ± 39

Replacing phenol in step 1 with 4-tertbutylphenol resulted in the same PMEM828 structure but with a tertbutyl substituent side chain causing a significant increase in viscosity from 1082 cP to 2442 cP. While the viscosity of BPMEM828 (EEW = 677 g mol^{-1}) is still applicable to SLA applications, the increased viscosity can be explained by the presence of the tertbutyl group on the tertbutyl methacrylate. The tertbutyl group adds bulky hindrance for the molecules to move and contains 9 additional hydrogen atoms. Studies have shown that viscosity can be predicted by the number of

hydrogen bonds within a system and when systems have additional hydrogens, a higher

viscosity is expected [89]. Due to the increase molecular weight, added steric hindrance,

and increase in intermolecular interactions, a higher viscosity is expected with

BPMEM828 compared to PMEM828.

4.2.4 Extent of Cure

Near-IR was employed to calculate the extent of cure values for each functional

group at each stage of the curing process for both PMEM828 and BPMEM828. Extents

of cure values are reported in Table 7.

Table 7

Extent of Cure via Near-IR of PMEM828 and BPMEM828 Systems at Various Stages of

Cure

Sample	Methacrylate Extent of Cure (%)		
	AM	AM FC	AM FC PC
PMEM828	87.9 ± 1.0	89.7 ± 1.9	90.0 ± 1.6
BPMEM828	86.0 ± 1.3	91.6 ± 1.3	92.7 ± 1.7
Sample	Oxirane Extent of Cure (%)		
	AM	AM FC	AM FC PC
PMEM828	0	85.7 ± 1.5	100
BPMEM828	0	62.7 ± 4.3	100
Sample	Amine Extent of Cure (%)		
	AM	AM FC	AM FC PC
PMEM828	40.8 ± 9.9	85.8 ± 3.0	91.1 ± 1.9
BPMEM828	35.2 ± 9.7	78.3 ± 8.4	89.8 ± 2.5

Changing the phenol use in step 1 of the 1P2S reaction to 4-tertbutyl phenol resulted in no significant change in the extent of cure of the methacrylate network at each stage of the curing procedure. After the AM step, the methacrylate network is the only chain polymerized during this step as indicated by the 0% cure of the oxirane functionality. Despite the 35-40% cure at the AM step for the primary amine, the oxirane peak of the IR spectra did not decrease indicating that the amount of epoxy rings in the system remained constant through the SLA step. This is expected as the AM step is performed at ambient temperatures and the epoxy-amine network requires heat to initiate the ring-opening polymerization mechanism [90]. After the post processing steps, the extent of cure of the methacrylate group increases because of the light exposure for 2 hours in the Form Cure to around 90% for both systems and maintains the same extent of cure after all curing processes. The extent of cure determined from the oxirane peak at 4530 cm^{-1} shows a cure of 85.7% for PMEM828 and 62.7% for BPMEM828. The amine extent of cure for both systems at this stage of the curing process fall between 78-85% which support the changes in oxirane peak at this step. BPMEM828 can be exhibiting a lower extent of cure across the epoxy-amine chain due to the higher extent of cure from the methacrylate network and the steric hindrance imposed from the bulky nature of the tert-butyl group. Both the fully cured methacrylate network and the nature of the substituent could lessen the ability of the epoxy functionality on the EM828 monomer to easily react with the primary amine on the Epikure W. Despite the differences in extent of cure for the epoxy-amine network after the AM FC step, both IPNs show similar extents of cure after the last post-processing step with 100% conversion of the epoxy and

58

approximately 90% conversion of the primary amine. DSC measurements were taken to confirm that each network was fully cured and shown in Figure 19.

Figure 18

DSC Thermograms of Cured PMEM828 and BPMEM828
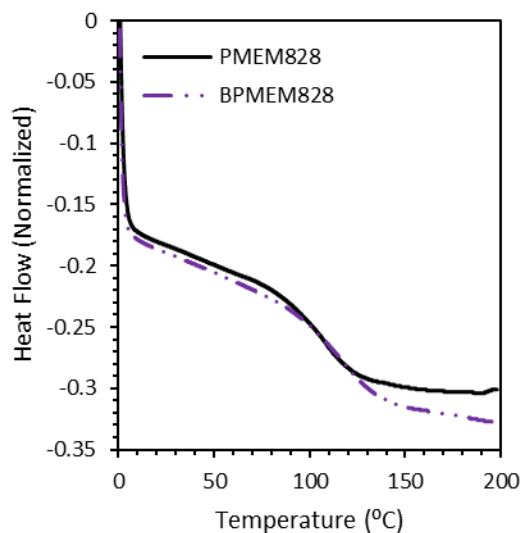
DSC thermograms between PMEM828 and BPMEM828 show no significant exotherms during the temperature ramp up to 200 $^{\circ}$C. Lack of exothermic reactions confirm that both IPNs were fully cured. Glass transition temperatures are visible in the thermograms but were not reported from DSC and instead will be reported from DMA results.

4.2.5 Polymer Properties

The resulting polymers were glassy and brown due to the Epikure W used as a curing agent. All processed polymers were evaluated with TGA to evaluate thermal degradation properties. Representative thermograms conducted under inert conditions of each fully cured IPN are displayed in Figure 20. The values of IDT, T_{50}, T_{max}, and char content were collected and reported in Table 8. Representative thermograms run under an oxidative atmosphere and the measured thermogravimetric values can be found in Appendix B.

Figure 19

TGA Thermograms and Respective 1ˢᵗ Derivative of PMEM828 and BPMEM828 in N_2
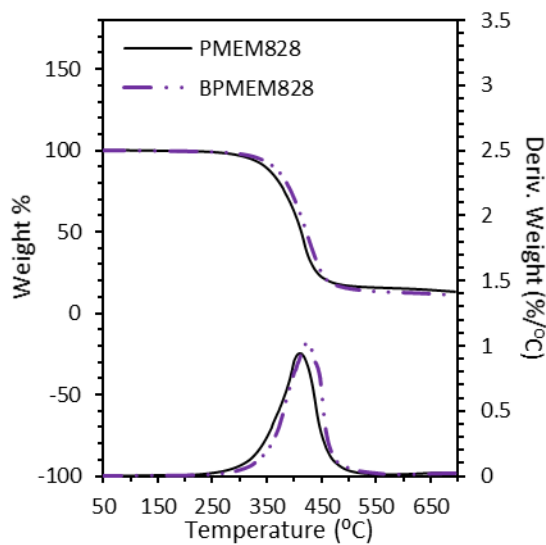
Table 8

Thermogravimetric Analysis Data of PMEM828 and BPMEM828 in N_2

Sample	IDT (°C)	$T_{50\%}$ (°C)	T_{max} (°C)	Char Content (%)
PMEM828	327 ± 9	417 ± 6	421 ± 5	12.1 ± 0.9
BPMEM828	331 ± 8	415 ± 9	419 ± 6	10.1 ± 0.5

By adding the tertbutyl group onto the phenol ring in the methacrylate network of the IPN, no effect was seen on any of the thermal degradation properties collected during TGA. All the temperatures determined to be of significant degradation marks were found to be within 2 °C of one another without any statistical significance. Similar trends were observed under oxidative conditions with the exception of the char content which is due to the char left over being completely combusted at higher temperatures [80].

The viscoelastic properties of both PMEM828 and BPMEM828 were measured with DMA. Thermograms shown in Figure 21 display representative storage moduli (E') and loss moduli (E'') while Figure 22 shows representative tan δ curves for both cured networks. All measured and calculated values found with DMA are reported in Table 9. Additional DMA data can be found in Appendix C.

Figure 20

DMA Thermograms of E' and E'' for all PMEM828 and BPMEM828
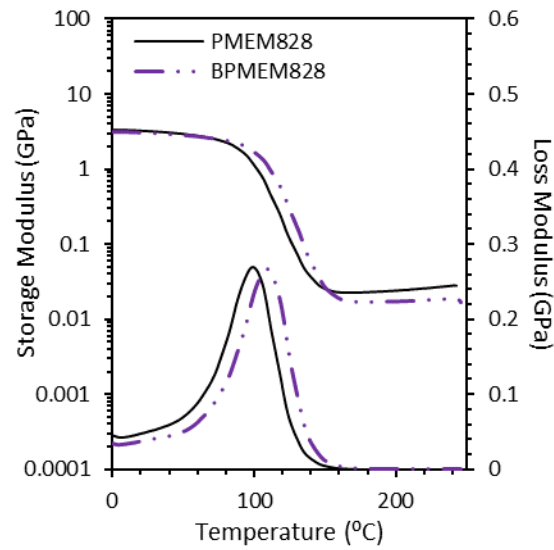
Figure 21

DMA Thermograms of Tan δ for all PMEM828 and BPMEM828
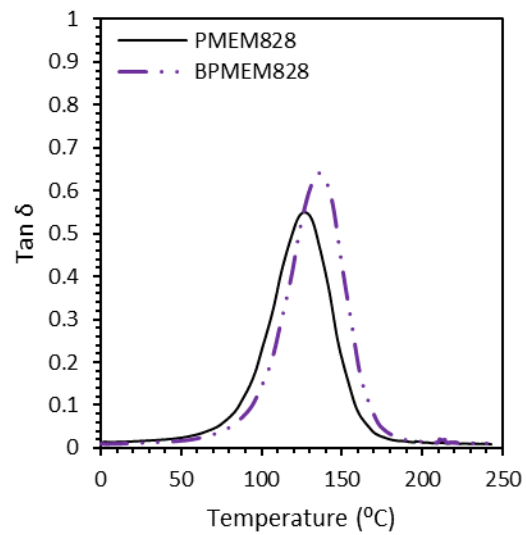
Table 9

Viscoelastic Data of PMEM828 and BPMEM828

Sample	E′ @ 25 °C (GPa)	Peak of E″ (°C)	Peak of Tan δ (°C)	M_c (g mol^{-1})	ρ @ 25 °C (g cm^{-3})
PMEM828	3.1 ± 0.2	99 ± 3	131 ± 3	499 ± 56	1.199 ± 0.001
BPMEM828	3.3 ± 0.1	108 ± 2	143 ± 2	818 ± 56	1.158 ± 0.001

Thermomechanical properties were compared between PMEM828 and BPMEM828 and were found to change with the addition of a tert-butyl substituent on phenol in the first step. The storage modulus marginally increased with the substitution of terbutylphenol for phenol in the 1P2S reaction indicating a slightly stiffer material at room temperature and agreed with literature values of *E′* for styrene-diluted VERs [68]. Both the peak of E″ and peak of tan δ increased from 99 °C to 108 °C and 131 °C to 143 °C, respectively. The increase in temperature at which the peak of the loss modulus occurs suggests that the addition of the tertbutyl substituent on the phenol in the first step altered the configuration between the methacrylate network and the epoxy-amine network to aid in the ability of the polymer to dissipate mechanical energy [91]. This is also reflected in the increase of the peak in the tan δ, which corresponds to the increase in loss modulus and consistent storage modulus. The peak of the tan δ can also signify T_g of the polymers. The rise in T_g can be explained due to the new side group present in BPMEM828 and the shape of the substituent. It has been observed in previous studies that T_g increases primarily in relation to local steric hindrance of segmental conformational motion and increased cohesive energy between chains [92], [93].

The shape of the tan δ curve for both IPNs have comparable widths but differ slightly in intensity. This implies comparable homogeneity between networks but different chain mobilities. The heightened peak intensity for the tan δ of BPMEM828 suggests increasing segmental chain motion between crosslinks with increasing chain length, or decreasing crosslink density [94]. This trend is reflected in the calculated M_c values for both IPNs. By adding the tert-butyl substituent to the phenyl methacrylate in the IPN, the effective molecular weight between crosslinks increases from 499 g mol^{-1} to 818 g mol^{-1}. The increase in M_c suggests that the addition of the tert-butyl group enhances the chain mobility of the methacrylate network allowing for potentially enhanced mechanical properties [33]. Despite the difference in molecular weight of 56 g mol^{-1} between reactants, the effective molecular weight between crosslinks increases by approximately 300 g mol^{-1}. This trend can be explained by assuming the molecular weight of a singular crosslink corresponds to 4 BPMEM828 monomer units. When comparing the M_c between PMEM828 and BPMEM828 the molecular weight should increase by roughly 4 tertbutyl substituents, which should increase the M_c by approximately 256 g mol^{-1}. This assumption could explain the viscoelastic trends between PMEM828 and BPMEM828, however a deeper look into how the network is forming would provide more clarity.

Mechanical properties for PMEM828 and BPMEM828 were quantified through compressive strength and fracture toughness. Representative stress-strain curves from compression testing for both IPNs are displayed in Figure 23. The maximum strength

reached at compressive failure and compressive modulus were evaluated and listed in

Table 10.

Figure 22

Stress-Strain Curves for PMEM828 and BPMEM828
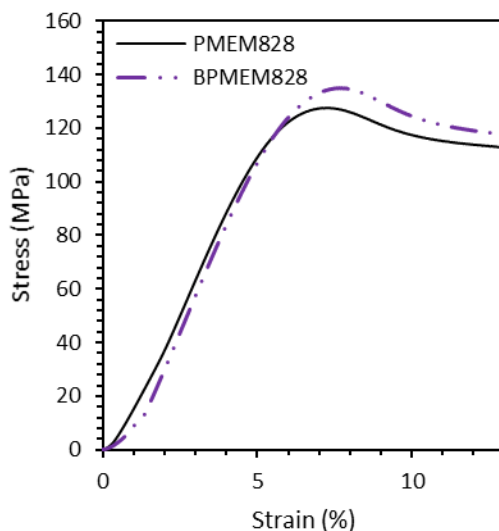
Table 10

Compression Testing Values PMEM828 and BPMEM828

Sample	Compressive Strength (MPa)	Compressive Modulus (MPa)
PMEM828	128 ± 5	2191 ± 461
BPMEM828	132 ± 3	2075 ± 146

Compression testing revealed that maximum compressive strength was slightly

improved with the addition of the tertbutyl group onto the methacrylate network of the

IPN. Despite the marginal increase in compressive strength, the difference in compressive modulus was found to be statistically insignificant. The compressive modulus is calculated by finding the slope of the initial linear region of the stress-strain curves [33]. Differences in compressive modulus will show changes in a materials behavior, however in this case the changes in methacrylate network do not affect the IPNs behavior in the glassy state.

Further structural analysis was performed through fracture toughness experiments. Representative load-displacement curves are presented in Figure 24. Critical strain energy release rate, G_{1C}, and plane-strain fracture toughness, K_{1C}, were also evaluated for both PMEM828 and BPMEM828 and listed in Table 11.

Figure 23

Load-Displacement Curves for PMEM828 and BPMEM828
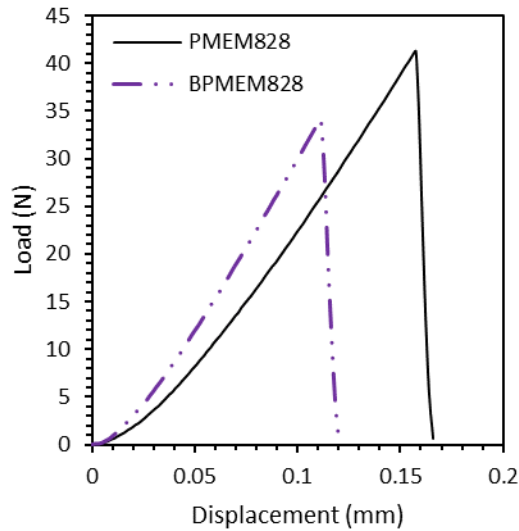
Table 11

Fracture Toughness K_{1C} and G_{1C} Values for PMEM828 and BPMEM828

Sample	G_{1C} (J/m²)	K_{1C} (MPa m$^{1/2}$)
PMEM828	171 ± 30	1.00 ± 0.09
BPMEM828	107 ± 37	0.53 ± 0.11

Changing phenol in step one of the 1P2S synthesis of IPN PMEM828 to 4-tertbutyl phenol dramatically reduced both G_{1C} and K_{1C}. Both formulations continued to display linear load and plastic deformation until failure exhibiting brittle behavior [95], [96]. By changing the monofunctional monomer of the methacrylate network and introducing a new side length with steric hindrance, the ability of the polymer to

67

withstand plastic deformation lessens at room temperature. Despite the intensity of the

tan δ peak increasing with the addition of the tert-butyl group on the phenyl methacrylate,

the increase in chain mobility does not always indicate good impact properties [97].

Impact properties are more so determined by which chain has greater mobility, namely

the main chain. In the case of BPMEM828, the main chain is more rigid at room

temperature as indicated by the increased storage modulus at 25 °C and increased T_g. The

increased storage modulus and T_g values indicates a stiffer, or more rigid, material at

room temperature which is reflected in the reduced fracture properties exhibited by

BPMEM828.

4.3 Modifying Step 2 of 1P2S

4.3.1 Introduction

The main goal of this section is to explore how altering the second step in the

coveted 1P2S synthesis scheme affects the thermal and mechanical performance of the

IPN. Epon828, which is partially methacrylated in the IPN, PMEM828, is brittle in nature

due to the aromaticity in its chemical structure. It has been found that by adding small

amounts of aliphatic epoxy copolymers to the neat resin, mechanical properties can be

improved without affecting thermal resistance. A commonly used aliphatic epoxy

copolymer is diluent HM68 due to its wetting out capabilities to enhance compatibility

between materials. Typically, diluents like HM68 are added to resin systems but in this

study select concentrations of Epon828 were replaced with HM68 to maintain the

aromaticity in the resin system and preserve the rigidity of the final IPN. Previous studies

have found that additions of <5% oftentimes resulted in a negligible effect but additions

of >50% negatively impacted resin and polymer properties [98], [99]. In this study, 10 wt% and 25 wt% of Epon828 were replaced with HM68 in the 1P2S synthesis of PMEM828 and evaluated via thermomechanical, thermogravimetric, compression, and fracture analysis to determine the effect of added aliphatic character.

4.3.2 Resin Rheology

The presence of HM68 did not change the observed Newtonian behavior of PMEM828 resin at either concentration. The viscosity of each resin was taken as an average of 3 steady state points at varying shear rates and shown in Table 12. Typically lower viscosities are preferred for SLA techniques to aid in processibility and most commercial SLA resins fall within 500 to 1500 cP at room temperature [3, 13]. PMEM828 is known to have a viscosity of 1172 ± 34 cP reported by Bassett et al [34]. While this viscosity falls well within the range of other SLA commercially relevant resins, lowering the viscosity can improve the resolution of the object produced with other rapid prototyping techniques.

Table 12

Viscosities of Resins at 25 ⁰C

Sample	Viscosity at 25 ⁰C (cP)
PM-EM828	1082 ± 30
PMEM828 w/ 10% HM68	585 ± 40
PMEM828 w/ 25% HM68	332 ± 32

The viscosities of each resin system were seen to decrease, as expected, with added HM68 as depicted in Figure 25. According to Hexion, substituting 10% of the viscosity reducing agent lowers the viscosity of Epon828 from approximately 11,000 cP to almost 3200 cP [98]. Replacing 10% of Epon828 with HM68 (EEW = 610 g mol^{-1}), reduced the viscosity of PMEM828 by nearly 45% and substituting 25% of Epon828 (EEW = 596 g mol^{-1}) with HM68, reduced the viscosity by ~70%. While the viscosity of PMEM828 with 25% HM68 is lower than typical available SLA resins, it will still be advantageous for any photosensitive resins because a low viscosity material will ensure a better flow which is required for rapid photocuring techniques at ambient temperatures [100].

4.3.3 Extent of Cure

Near-IR was employed to calculate the extent of cure values for each functional group at each stage of the curing process for all resin systems. Extents of cure values are reported in Table 13.

Table 13

Extent of Cure via Near-IR of IPN With HM68 Systems at Various Stages of Cure

Sample	Methacrylate Extent of Cure (%)		
	AM	AM FC	AM FC PC
PMEM828	87.9 ± 1.0	89.7 ± 1.9	90.0 ± 1.6
PMEM828 w/ 10% HM68	89.8 ± 0.8	93.8 ± 1.3	91.8 ± 1.2
PMEM828 w/ 25% HM68	86.4 ± 2.6	93.3 ± 2.7	91.3 ± 1.8
Sample	Oxirane Extent of Cure (%)		
	AM	AM FC	AM FC PC
PMEM828	0	85.7 ± 1.5	100
PMEM828 w/ 10% HM68	0	75.1 ± 5.5	100
PMEM828 w/ 25% HM68	0	81.2 ± 10.9	100
Sample	Amine Extent of Cure (%)		
	AM	AM FC	AM FC PC
PMEM828	40.8 ± 9.9	85.8 ± 3.0	91.1 ± 1.9
PMEM828 w/ 10% HM68	28.1 ± 5.6	79.1 ± 3.4	92.9 ± 0.8
PMEM828 w/ 25% HM68	27.3 ± 7.8	74.7 ± 3.8	95.5 ± 2.5

Substituting 10-25% Epon828 with HM68 had little to no effect on the conversion of methacrylate, oxirane, and amines. As seen, after AM step, the methacrylate functionality is the only component of each IPN that is cured. The methacrylate network is formed because of photopolymerization which is initiated by the presence of the photo initiator TPO and a light source, which is the visible light laser in the Form2 SLA printer. Despite adding varying concentration of the viscosity reducing agent, the methacrylate extent of cure after the AM step for all resins is 85-90%. The oxirane conversion after the AM step remains unchanged with the addition of HM68 because the method of polymerization between the epoxy terminus and the amine require heat to initiate the ring-opening mechanism. Despite the requirement of heat to form the epoxy-amine

71

network present in PMEM828 and the subsequent systems, near-IR reveals amine conversion of 25-40% between all systems. While the amine conversion is significantly higher than the oxirane conversion, the near-IR reveals that the epoxy-amine network has not been formed during this step but the primary amine from the Epikure W, present at 5000 cm^{-1} has converted to a secondary amine that is shown in the peak at 6600 cm^{-1}. Potential explanations for this phenomenon could be attributed to the shelf life of the amine curing agent used throughout the study, limitations to near-IR, as well as possible interactions between the primary amine on Epikure W and other reactive components of the 1P2S synthesized resin.

After the FC step, the methacrylate extent of cure increased to 90-94% due to the irradiation of the UV/ visible light in the Form Cure for an additional 2 hours after print and remained at 90-92% cured after the thermal post cure step. It is safe to assume that any decrease in extent of cure for the methacrylate network after the thermal post cure step is due to limitations of near-IR and not an actual decrease in methacrylate conversion.

The epoxy-amine network was initiated during the Form Cure step of the curing procedure due to the post-processing temperature of 80 ^{o}C for 2 hours which is well within the range of temperatures required to initiate typical ring-opening polymerization mechanisms [68], [101], [102]. Conversion of both the oxirane and primary amine peaks agree with one another by showing extents of cure between 75-85% after FC. The final curing step of thermal curing at a temperature of 180 ^{o}C in attempt to fully convert the epoxy-amine network shows 100% conversion of the oxirane peak with 90-95%

conversion of the primary amine. DSC measurements were taken to confirm that each

network was fully cured and representative thermograms are shown in Figure 26.

Figure 24

DSC Thermograms of Cured IPNs With HM68
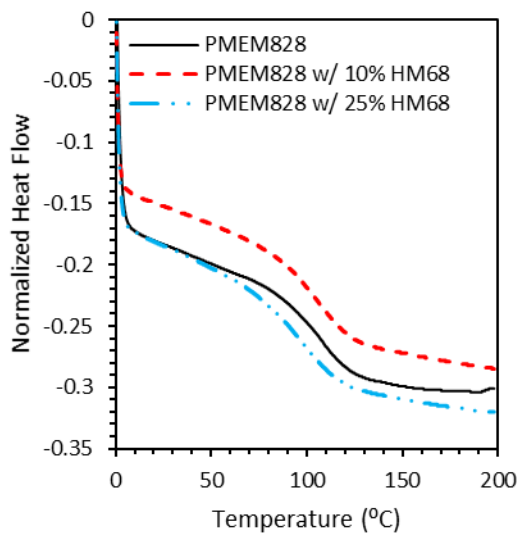
DSC thermograms reveal no appreciable exotherms in any of the IPN networks

conducted in the study. Lack of exothermic reactions confirm that each polymer tested in

this section of the study was fully cured. Glass transition temperatures are visible in the

thermograms but were not reported from DSC but instead are reported from DMA

results.

4.3.4 Polymer Properties

All polymers cured during this study were analyzed for thermogravimetric properties, viscoelastic properties, and mechanical properties. The thermogravimetric properties of each IPN formulation were analyzed via TGA in both inert (N_2) and oxidative (air) environments. Representative thermograms of each IPN under inert conditions are shown in Figure 27. Representative thermograms for each polymer in an oxidative atmosphere are displayed in Appendix B. The IDT, $T_{50\%}$, T_{max}, and char content for each cured polymer is shown in Table 14.

Figure 25

TGA Thermograms and Respective 1st Derivative of All IPNs With HM68 in N_2
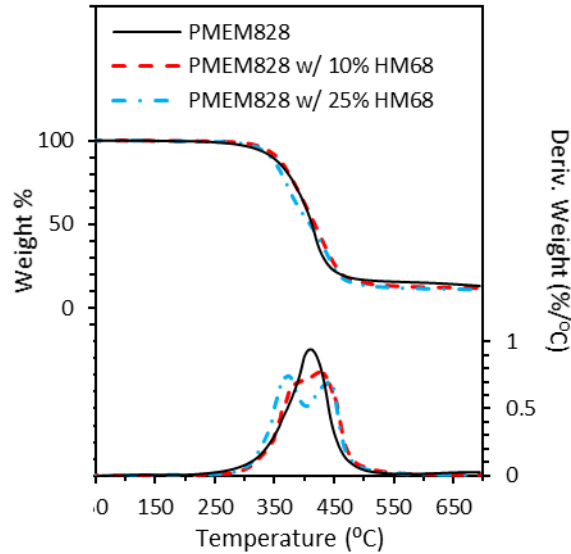
Table 14

Thermogravimetric Analysis Data of IPNs With HM68 in N_2

Sample	IDT (°C)	$T_{50\%}$ (°C)	T_{max} (°C)	T_{max2} (°C)	Char Content (%)
PMEM828	327 ± 9	417 ± 6	421 ± 5	-	12.1 ± 0.9
PMEM828 w/ 10% HM68	331 ± 2	417 ± 1	423 ± 5	-	12.7 ± 0.5
PMEM828 w/ 25% HM68	324 ± 3	409 ± 1	372 ± 2	435 ± 6	12.0 ± 0.7

Thermogravimetric analysis revealed that the thermal degradation properties of the IPNs were not affected with the addition of HM68. All IPNs showed an IDT of upward of 330 °C, $T_{50\%}$ and T_{max} around 420°C, and a char yield around 12% in an inert atmosphere. The only significant discrepancy across TGA was found in the 1st derivative thermogram of the PMEM828 w/ 25% HM68. The first derivative curve of the IPN with the higher concentration of HM68 revealed two distinct decomposition rates in the cured IPN. The additional decomposition point illustrates the presence of the lower molecular weight polymer chain that is present with the addition of HM68. The higher addition of HM68 is likely to reduce the amount of crosslinking present in the IPN and it has been found that with lighter crosslinked polymers thermal degradation can begin at lower temperatures [103]. Similar trends were observed under oxidative conditions with the exception of the char content which is due to the char left over being completely combusted at higher temperatures [80].

The viscoelastic properties of each IPN were quantified using DMA. Thermograms shown in Figure 28 display representative storage moduli (E') and loss moduli (E'') and Figure 29 shows representative tan δ curves for all cured polymers. All

measured and calculated values found with DMA are listed in Table 15. Additional DMA

data can be found in Appendix C.

Figure 26

DMA Thermograms of E' and E'' for All IPNs With HM68
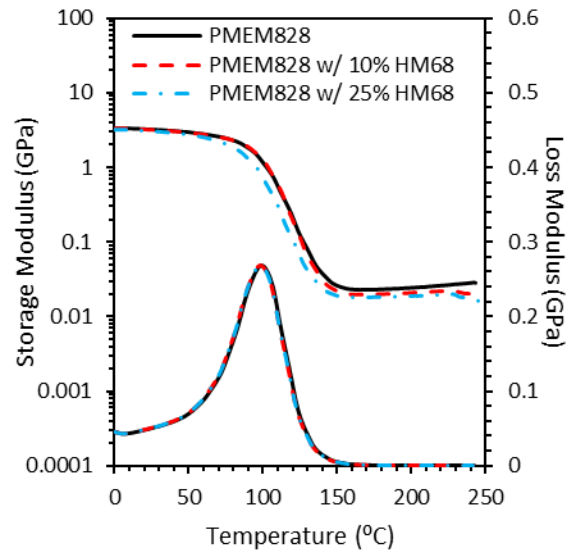
Figure 27

DMA Thermograms of Tan δ for All IPNs With HM68
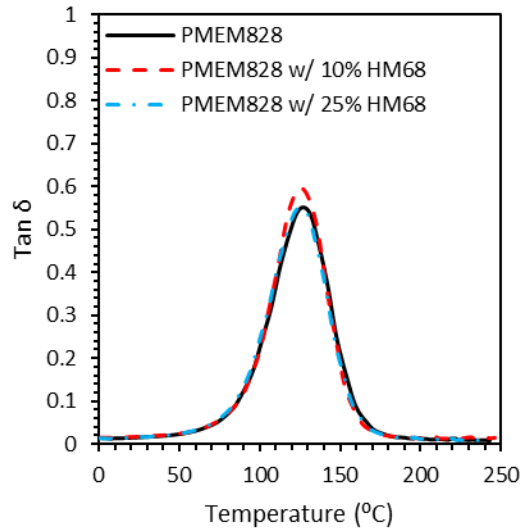
Table 15

Viscoelastic Data of All IPNs With HM68

Sample	E′ @ 25 °C (GPa)	Peak of E″ (°C)	Peak of Tan δ (°C)	M_c (g mol^{-1})	ρ @ 25 °C (g cm^{-3})
PMEM828	3.1 ± 0.2	99 ± 3	131 ± 3	499 ± 56	1.199 ± 0.001
PMEM828 w/ 10% HM68	3.3 ± 0.2	98 ± 5	129 ± 6	633 ± 34	1.197 ± 0.002
PMEM828 w/ 25% HM68	3.1 ± 0.1	97 ± 1	131 ± 2	735 ± 51	1.186 ± 0.011

DMA for IPNs with varying levels of HM68 were showed to have minimal change in viscoelastic properties. The storage modulus measured at 25°C remained around 3 GPA which agreed with what has previously been reported in the literature

regarding styrene-diluted VERs [68]. The T_g for these polymers were reported with both the peak of the loss modulus and the peak of the tan δ. Both values were used in order to provide a conservative estimate as well as a higher limit value for the point where the polymer transitions from a glassy to a rubbery state [67]. In general, the T_g for each system was reported as 98 °C from E'' and 130 °C from the peak of the tan δ which supports the viscoelastic data reported previously regarding styrene-diluted VERs [68].

The shapes of the DMA curves for the tan δ can draw insight into how the structure of each IPN changes with the addition of HM68. The width of the tan δ changes with the heterogeneity of the polymer network and the height of the tan δ changes as the mobility of the polymer chain increases [104], [105]. From Figure 29, the width of the tan δ curve remains constant despite the increasing level of HM68 indicating that the heterogeneity of the polymer network does not change. The height of the tan δ curve slightly increases at the maximum concentration of HM68. The increased height of the tan δ curve suggests that the HM68, at that level of loading, slightly increased the chain mobility of the crosslinked network. However, at this level of concentration, the difference is statistically insignificant and remains consistent with the original PMEM828 system.

The M_c was calculated using the Theory of Rubbery Elasticity. Despite negligible differences between extents of cure and thermal degradation, the IPN becomes significantly less crosslinked with the addition of HM68. Typically, other studies have noticed that with adding a multifunctional aliphatic epoxy with a lower EEW, the cross-

link density will increase because there is a shorter distance between crosslinks [106]. However, these past studies were only conducted on strictly epoxy-amine networks. This study offers an additional variable to consider with the presence of the methacrylate network formed with the phenyl methacrylate and the methacrylate functionality of the di-functional epoxies. During the AM step, the methacrylate network is formed via free-radical polymerization. The epoxy-amine network does not form until the subsequent post processing steps where heat is applied to the system. Therefore, the pre-existing methacrylate network affects the imbibement of the secondary network which can greatly reduce the degree of crosslinking [25]. While we would expect to see reduced extents of cure to support this claim, we do not. This can be explained by the inability to predict the distribution of products formed in the 2nd step of 1P2S synthesis of PMEM828. While we assume full conversion to EM828, there is unreacted Epon828, EM828, and vinyl ester828 (VE828), where both epoxies have been converted to methacrylate functionalities. This becomes more complex with the addition of HM68. Due to the differences in reactivities between methacrylates and epoxies on different monomers, the formation of IPNs can vary greatly. This variance, along with the sequential curing procedure, contributes to the reduction of crosslink density with increasing concentration HM68. Conversely, the densities of the IPN systems decrease with increasing concentrations of HM68. This trend, while statistically insignificant, can be explained by introducing a diluent of lower molecular weight into the IPN, which directly reduces the density of the cured polymer.

Mechanical properties of all IPNs were evaluated based on compressive strength

and fracture toughness. Representative stress-strain curves from compression testing for

all IPN resins are displayed in Figure 30. The maximum strength reached at compressive

failure and compressive modulus were evaluated and listed in Table 16.

Figure 28

Stress-Strain Curves for All IPNs With HM68
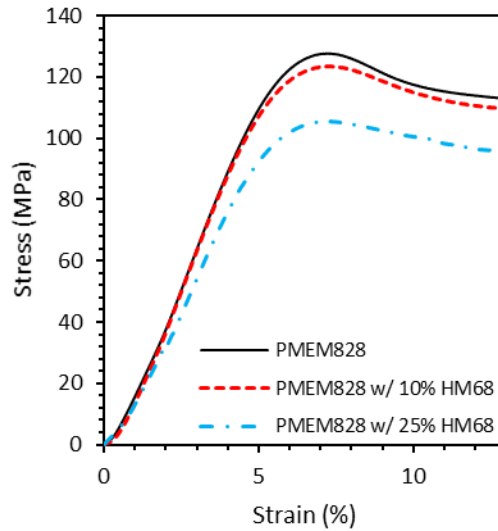
Table 16

Compression Testing Values for All IPNs With HM68

Sample	Compressive Strength (MPa)	Compressive Modulus (MPa)
PMEM828	128 ± 5	2191 ± 461
PMEM828 w/ 10% HM68	123 ± 3	1887 ± 380
PMEM828 w/ 25% HM68	106 ± 5	1697 ± 236

Compressive strength and compressive modulus decrease as more HM68 is introduced into the system. This is consistent with what has been reported in literature where compressive modulus decreases with the addition of diluents by Zhang et al [107]. PMEM828 exhibited maximum compressive strength of 128 MPa with an average compressive modulus of 2191 MPa. When adding 10% HM68, the compressive strength of the IPN lowered to 123 MPa and the compressive modulus followed the same trend by decreasing to 1887 MPa. While 10 wt% of the aliphatic epoxy co-polymer reduced the compressive properties of the IPN, the changes were not statistically significant. However, adding 25 wt% HM68 reduced the compressive strength of the IPN to 106 MPa and the compressive modulus to 1697 MPa. At this loading of HM68, the change in compressive properties was statistically significant. In previous studies, lower concentration of diluent (<5%) into neat epoxy-amine systems have no effect on compressive modulus, or the stiffness of a material. However, at more significant additions of diluent (50-100%), modulus as well as maximum yield stress decreases [99]. Urbanczewski- Espuche et al. conducted a study on blends of bisphenol A diglycidyl ether with aliphatic diepoxy diluents that were crosslinked with cycloaliphatic diamines exhibited similar behavior to the trends discerned in this study. Ultimately, they found that chain flexibility was the primary parameter to effect yield behavior of polymers and chain flexibility was found to increase with the addition of aliphatic diepoxy diluent [99]. These findings were consistent PMEM828 and increasing amounts of HM68. Due to the flexibility of the aliphatic diluent, the introduction of HM68 to PMEM828 promotes the mechanism of plastic deformation and the ability of defects to propagate.

81

Further structural analysis was performed through fracture toughness experiments. Representative load-displacement curves are displayed in Figure 31. Critical strain energy release rate, G_{1C}, and plane-strain fracture toughness, K_{1C}, were also evaluated for all IPN formulations and displayed in Table 17.

Figure 29

Load-Displacement Curves for All IPNs With HM68
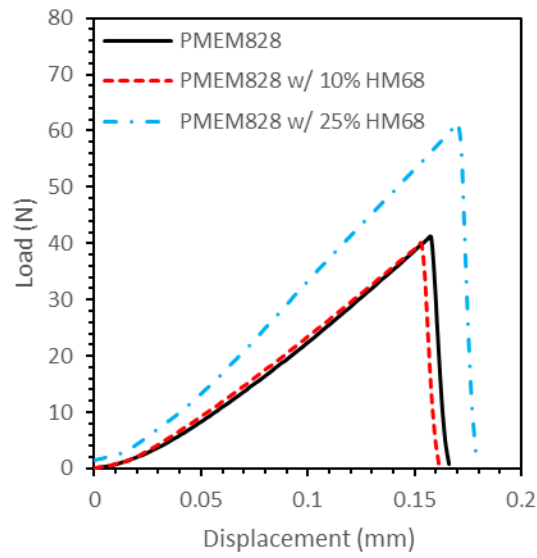
Table 17

Fracture Toughness K_{1C} and G_{1C} Values for All IPNs With HM68

Sample	G_{1C} (J/m^2)	K_{1C} (MPa m$^{1/2}$)
PMEM828	171 ± 30	1.00 ± 0.09
PMEM828 w/ 10% HM68	170 ± 49	0.67 ± 0.1
PMEM828 w/ 25% HM68	282 ± 111	1.10 ± 0.44

The 10 wt% addition of HM68 did not statistically impact the G_{1C} of the unmodified PMEM828 polymer which is consistent with previous studies that have added low amounts of diepoxy diluents [99]. However, with 25 wt% of HM68 the G_{1C} of PMEM828 increased from 171 J/m^2 to 282 J/m^2 which is an increase of approximately 65% in critical strain energy release rate to compare to G_{1C} of conventional styrene-diluted VERs (255 J m^{-2}) [68]. Despite such a large difference in G_{1C}, the K_{1C} remained unaffected with the addition of 25 wt% HM68 and decreased with 10 wt% HM68. Adding small amounts of diepoxy diluents such as HM68 can limit the ability of a polymer to plastically deform but when added in larger quantities can significantly aid in the ability of the polymer to plastically deform. It has been shown in many studies that the toughness of a material is not dependent on the crosslinks of the polymer network but the flexibility of the polymer chain [99], [108], [109]. In the case of PMEM828, the crosslink density decreases as more HM68 is introduced into the IPN, but the flexibility of the chain is not optimized until larger amounts of aliphatic character are present within the network.

Chapter 5

Conclusions and Future Work

5.1 Conclusions

This thesis aimed to change components in the 1P2S synthesis of PMEM828 to make different IPNs with a higher degree of aliphatic character. By adding more aliphatic character to the IPN, this work hypothesized that mechanical performance and processing would be improved while maintaining thermal stability. This thesis also accomplished removing discontinued chromium-based catalyst AMC-2 from the second step of the 1P2S synthesis without changing the shelf life of the resin or the final measured properties of the cured polymer.

Phenol in step 1 was replaced with 4-tertbutylphenol to produce tertbutyl methacrylate and methacrylic acid. Methacrylic acid would then partially methacrylate di-epoxy Epon828 in step 2 to form the dual functional monomer, EM828. This dual functional monomer would participate with the tertbutyl methacrylate in step 1 and amine curing agent Epikure W to form an IPN manufactured by SLA and subsequently post processed. Adding the tertbutyl substituent to the methacrylate network of the IPN resulted in an increased resin viscosity, a higher T_g, larger M_c, a lower density, and lower fracture toughness while exhibiting the same degree of cure. All final values for the methacrylate network resulted in extents of cure above 90% for both IPNs with epoxy functionality reaching full conversion. DSC thermograms further supported extents of cure values with no significant exotherms. The viscosity of PMEM828 doubled from

1082 cP to over 2442 cP with the addition of the tertbutyl substituent in the methacrylate network. Changing phenol to tertbutyl phenol also changed the properties of the cured polymer. DMA revealed that BPMEM828 had a T_g over 10$^\mathbf{o}$C higher than PMEM828. DMA showed an increase in M_c from 499 g mol^{-1} to 818 g mol^{-1} with the addition of the tertbutyl substituent. Comparing mechanical properties of the two IPNs resulted in no significant change to compressive modulus of around 2100 MPa and a slightly higher strength at yield for BPMEM828. Despite the marginal increase in compressive strength from 128 MPa to 132 MPa, the fracture toughness found for BPMEM828 decreased with the additional aliphatic substituent. PMEM828 exhibited G_{1C} and K_{1C} values of 171 J m^{-2} and 1.00 MPa m$^{1/2}$ respectively while BPMEM828 showed G_{1C} and K_{1C} values of 107 J m^{-2} and 0.53 MPa m$^{1/2}$, indicating that the addition of the tertbutyl substituent imparted a significant amount of rigidity to the initially formed polymer chain.

The second part of this study focused on replacing various amounts of Epon828 in the second step of the 1P2S synthesis with viscosity reducing agent HM68. This substitution was performed at 10 and 25% based on the weight of Epon828. With the addition of HM68 to the IPN PMEM828, thermal properties were maintained while mechanical performance properties were improved. This was shown through consistent extents of cure across methacrylate, epoxy, and amine functionalities. Methacrylate extents of cure after post processing steps were 90% or greater with complimenting full conversion of epoxy. These findings were further supported by DSC thermograms which displayed no residual exotherms suggesting a fully cured polymer network. DMA revealed storage moduli above 3.0 GPa for all formulations in this study and a T_g of

approximately 130 ℃ signified by the peak of the tan δ. While DMA showed that the thermal properties of each network were unchanged with the inclusion of HM68, the M_c steadily increased as a function of added HM68. A calculated M_c for PMEM828 was found to be 499 g mol^{-1}, however the crosslink density of the IPN decreased with added HM68 content. An addition of 10 wt% HM68 increased the M_c to 633 g mol^{-1} while an added 25 wt% HM68 increased the M_c to 735 g mol^{-1} indicating a reduction in crosslink density. This decrease in crosslink density can be explained by the predetermination of the polymer structure from the initially formed methacrylate network as well as the inability to determine the distribution of methacrylated functionalities in the second step. This unknown does not deplete the mechanical performance of the final cured polymer properties. Compression testing revealed that compressive modulus decreased with the addition of HM68 from about 2100 MPa to nearly 1700 MPa. This reduction in compressive properties was echoed by the decreasing compressive stress at yield with the addition of HM68. PMEM828 yielded at 128 MPa while 10 wt% HM68 and 25 wt% HM68 lowered the compressive stress at yield to 123 and 106 MPa respectively. A decrease in compressive properties can be explained by introducing a greater degree of plastic deformation within the network with the addition of HM68 but it still hindered by the aromaticity associated with PMEM828. Fracture toughness showed an increase in polymer performance by increasing the G_{1C} and K_{1C} from 171 J m^{-2} and 1.00 MPa m$^{1/2}$ to 282 J m^{-2} and 1.10 MPa m$^{1/2}$, respectively, with an addition of 25 wt% HM68. Adding 10 wt% HM68 showed no statistical change in fracture toughness with G_{1C} and K_{1C} from 170 J m^{-2} and 0.69 MPa m$^{1/2}$.

What we can gather from this data is that adding more aliphatic character to the IPN produced with 1P2S methodology can enhance mechanical properties while maintaining thermal stability if done strategically. Due to the sequential curing procedure inherent to the IPN formulations made with the 1P2S reaction schema, the methacrylate network is known to form 1st, followed by the formation of the epoxy-amine network. Therefore, the methacrylate network structure formed during SLA will greatly impact the structural integrity of the secondary network by hindering the mobility of the epoxy terminus of the dual functional monomer. This strategy suggests that if aliphatic character is added to the firstly formed methacrylate network, the additional substituent can inhibit the ability of the epoxy link with the amine due to steric hindrance. However, if aliphatic character is strategically added to the secondary network of the IPN, mechanical performance can be improved without affecting thermal properties to rival mechanical properties of conventional styrene-diluted VERs which cannot be manufactured through SLA due to the volatility of styrene as a hazardous air pollutant [68].

5.2 Future Work

5.2.1 Changing 1P2S

IPNs have proven to be an asset to many different industries for their high-performance capabilities. The 1P2S synthesis of PMEM828 and other IPNs is an attractive methodology because there are no required washing steps to isolate the final product and the procedure is easy to scale up for industry. Unfortunately, there are still many unknowns that exist within this reaction that would be valuable to investigate

further and perhaps improve to be a more viable option for commercial and military

applications.

A short shelf-life study was performed in this work to evaluate the effectiveness

in AMC-2 catalyst in the second step of the 1P2S synthesis. While successfully ruling out

the need for the chromium-based catalyst, other concerns were identified during this

study. The tertiary amine DMAP used in the first step also causes epoxy

homopolymerization when Epon828 is introduced into the system. Despite partially

methacrylating Epon828 to form EM828, an unreacted epoxy still exists within the

system which will readily homopolymerize under ambient conditions due to the presence

of DMAP. While epoxy-homopolymerization can be delayed by storing at 0 ^{o}C for a

reasonable amount of time, this problem could ultimately be avoided with the use of

another catalyst to preserve the 1P2S methodology. In recent studies, iodine has been

found to promote the acetylation of alcohols at room temperature regardless of

orientation on phenolic [110], [111]. Perhaps, iodine could promote the esterification of

phenol with methacrylic anhydride at elevated temperatures of 50°C or even higher

before promoting polymerization. Alternative reagents could be considered in place of

methacrylic anhydride to promote reactivity in exchange for a longer shelf life. This

could potentially introduce more hazards when synthesizing the resin due to the volatility

of methacryloyl chloride but completely prevent epoxy homopolymerization to occur

within the resin system. Another alternative to increase the shelf life of the final

formulated IPN resin would be to forgo the 1P2S synthesis scheme and adapt a one-pot-

one-step synthesis. This would involve combining Epon828 and methacrylic acid

together at elevated temperatures in the presence of an alternate catalyst that would

effectively facilitate the epoxy-carboxyl reaction to partially methacrylate Epon828

without risk of encouraging epoxy homopolymerization. Possible alternative catalysts to

consider are triphenyl phosphine in a combination with triphenyl antimony, metal

chelates such as zinc chelate or magnesium chelate, and metal salts [77], [112]. Once the

dual functional monomer is synthesized, reactive diluents such as phenyl methacrylate

can be purchased and mixed in at a stoichiometric ratio. Alternative reactive diluents can

also be combined to achieve enhanced mechanical properties such as cardanol

methacrylate (GX-7201) or benzyl methacrylate as pictured in Figure 32. This would

make the synthesis and shelf life of such IPNs more viable for military and industrial

applications.

Figure 30

Manufactured Reactive Diluents for Potential Use in Future IPNs
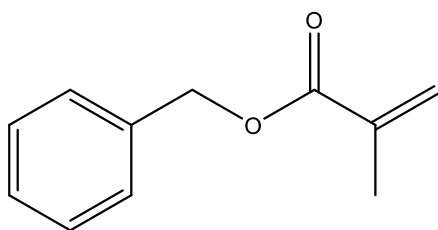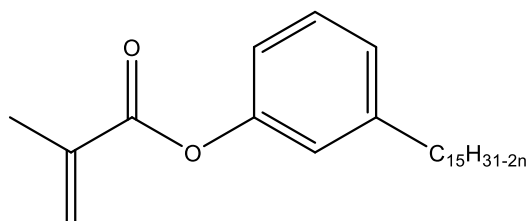
Benzyl Methacrylate   Cardanol Methacrylate (GX-7021)

5.2.2 Additional Analysis to Further Understand 1P2S

Additionally, this work was performed in a systematic order to determine structure relationships between chemical reagents and final polymer properties. A final extension of the work could be to combine all additional aliphatic components to find the final capabilities of the cured IPN. This was preliminarily done by synthesizing BPMEM828 w/ 25 wt% HM68 via 1P2S methodology. Each resin was evaluated for viscosity at 25 ^{o}C using a shear rate that was ramped logarithmically increasing from 1 to 100 s^{-1} and decreasing from 100 to 1 s^{-1}. Viscosity values were displayed in Table 18.

Table 18

Viscosities of BPMEM828 and BPMEM828 w/ 25 wt% HM68 Resins at 25 ^{o}C

Sample	Viscosity at 25 ^{o}C (cP)
BPMEM828	2442 ± 39
BPMEM828 w/ 25 wt% HM68	544 ± 18

Incorporating 25 wt% HM68 revealed a dramatic decrease in viscosity from 2442 cp to 544 cp. The reduction in viscosity will aid in processing BPMEM828 w/ HM68 via SLA and also reduce manufacturing costs with the inclusion of HM68. Each resin was sequentially cured with SLA and 2 post processing steps as mentioned in Chapter 3 in efforts to improve mechanical performance while maintaining thermal properties. The resulting polymers were evaluated for fracture toughness by calculating G_{IC} and K_{IC}. Representative load displacement curves for BPMEM828 and BPMEM828 w/ 25 wt%

HM68 are presented in Figure 33. The corresponding G_{1C} and K_{1C} values are reported in Table 18.

Figure 31

Load-Displacement Curves for BPMEM828 and BPMEM828 with 25 wt% HM68
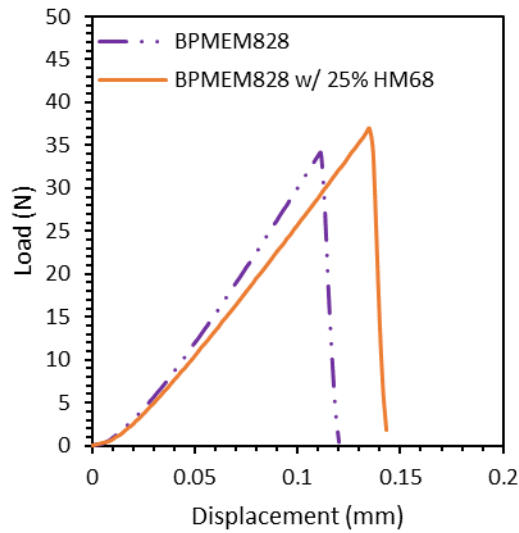
Table 19

Fracture Toughness K_{1C} and G_{1C} Values for BPMEM828 and BPMEM828 with 25% HM68

Sample	G_{1C} (J/m^2)	K_{1C} (MPa m$^{1/2}$)
BPMEM828	107 ± 37	0.53 ± 0.11
BPMEM828 w/ 25 wt% HM68	155 ± 29	0.63 ± 0.08

Fracture analysis of BPMEM828 and BPMEM828 with 25 wt% HM68 revealed a similar trend that was identified with PMEM828 and HM68. With higher content of aliphatic viscosity reducing agent HM68, the fracture toughness of BPEM828 increased and viscosity decreased to a more appropriate viscosity for SLA applications. This was not to the same degree that was observed for PMEM828 with 25% HM68, hence the need for additional analysis. We can assume that the bulky tertbutyl substituent on tertbutyl methacrylate could impose the same steric hindrance with the HM68 as with neat EM828, leading to a less significant change than PMEM828. However, additional analysis of how the network forms during cure, could frame a more definitive narrative for what is happening structurally within the IPN.

Kinetic studies for polymers have been an area of interest since the late 1800s when Musculus and Meyers studied the diffusion rates of the polymeric forms of simple sugars [74]. Fortunately, kinetic studies have evolved to incorporate many different instruments and analytical methods to determine reaction rates of forming polymers to study structure development as well as phase morphology of various polymer networks. Araujo and colleagues used DMA and modulated temperature DSC to assess the effect of reaction conditions on the formation of IPNs consisting of acrylate and epoxy functionalities and respective polymer properties [113]. Other teams have used FTIR, DSC, and gel time determine to discern the kinetics of network formation to better understand the a different epoxy-acrylate system [114]. Reaction kinetics has also been successfully evaluated by photodifferential scanning calorimetry to specifically observe the epoxy functionality and polymerization behavior of select IPN systems [24], [115].

These types of analytical techniques can also be nicely complimented with the addition of phase morphology study which can heavily influence the physical and mechanical properties because of the dual crosslinked nature of IPNs [25]. IPN morphology can be studied by different microscopy techniques like optical microscopy and transfer electron microscopy to observe the compatibility and dispersity of phase domains [25]. While phase separation was not observed in this work, phase separation might be occurring at the microscale or nanoscale which would be observed with different techniques. Other approaches have been used in the past to also evaluate the phase domains and microheterogeneity of IPNs through small-angle X-ray scattering and small-angle neutron scattering [116], [117]. Finding major discrepancies in phase domains can lead to phase separation which is a common occurrence in sequentially cured IPNs.

References

[1] S. Kumar, *Additive Manufacturing Processes*, 1st ed. 2020 edition. Cham: Springer, 2020.

[2] M. K. Thompson *et al.*, "Design for Additive Manufacturing: Trends, opportunities, considerations, and constraints," *CIRP Ann.*, vol. 65, no. 2, pp. 737–760, Jan. 2016, doi: 10.1016/j.cirp.2016.05.004.

[3] D. Bourell and J. Beaman, "Chronology and Current Processes for Freeform Fabrication," *J. Jpn. Soc. Powder Powder Metall.*, vol. 50, pp. 981–991, Nov. 2003, doi: 10.2497/jjspm.50.981.

[4] "Global Additive Manufacturing Market Generated $12 Billion Revenue in 2020, and is Forecast to Reach $78 Billion by 2028," *Researchandmarkets.com*, Sep. 14, 2020. https://www.businesswire.com/news/home/20200914005395/en/Global-Additive-Manufacturing-Market-Generated-12-Billion-Revenue-in-2020-and-is-Forecast-to-Reach-78-Billion-by-2028---ResearchAndMarkets.com (accessed Nov. 29, 2021).

[5] "New Wohlers Report 2021 Finds 7.5% Growth in Additive Manufacturing Industry Despite Pandemic," Wohlers Associates, Mar. 2021. Accessed: Nov. 29, 2021. [Online]. Available: https://wohlersassociates.com/press83.html

[6] I. Gibson, D. Rosen, B. Stucker, and M. Khorasani, *Additive Manufacturing Technologies*, 3rd ed. 2021 edition. Cham, Switzerland: Springer, 2020.

[7] J. R. C. Dizon, A. H. Espera, Q. Chen, and R. C. Advincula, "Mechanical characterization of 3D-printed polymers," *Addit. Manuf.*, vol. 20, pp. 44–67, Mar. 2018, doi: 10.1016/j.addma.2017.12.002.

[8] R. Quintana, J.-W. Choi, K. Puebla, and R. Wicker, "Effects of build orientation on tensile strength for stereolithography-manufactured ASTM D-638 type I specimens," 2010, doi: 10.1007/S00170-009-2066-Z.

[9] P. F. Jacobs, *Rapid Prototyping & Manufacturing: Fundamentals of Stereolithography*. Society of Manufacturing Engineers, 1992.

[10] P. J. Halley and G. A. George, *Chemorheology of Polymers: From Fundamental Principles to Reactive Processing*. Cambridge: Cambridge University Press, 2009. doi: 10.1017/CBO9780511581403.

[11] E. Andrzejewska, "Photopolymerization kinetics of multifunctional monomers," *Prog. Polym. Sci.*, vol. 26, no. 4, pp. 605–665, May 2001, doi: 10.1016/S0079-6700(01)00004-1.

[12] J. V. Crivello and E. Reichmanis, "Photopolymer Materials and Processes for Advanced Technologies," *Chem. Mater.*, vol. 26, no. 1, pp. 533–548, Jan. 2014, doi: 10.1021/cm402262g.

[13] J. V. Crivello, S. Rajaraman, W. A. Mowers, and S. Liu, "Free radical accelerated cationic polymerizations," *Macromol. Symp.*, vol. 157, no. 1, pp. 109–120, 2000, doi: 10.1002/1521-3900(200007)157:1<109::AID-MASY109>3.0.CO;2-Y.

[14] M. Sangermano, N. Razza, and J. V. Crivello, "Cationic UV-Curing: Technology and Applications," *Macromol. Mater. Eng.*, vol. 299, no. 7, pp. 775–793, 2014, doi: 10.1002/mame.201300349.

[15] A. C. Weems, K. R. Delle Chiaie, R. Yee, and A. P. Dove, "Selective Reactivity of Myrcene for Vat Photopolymerization 3D Printing and Postfabrication Surface Modification," *Biomacromolecules*, vol. 21, no. 1, pp. 163–170, Jan. 2020, doi: 10.1021/acs.biomac.9b01125.

[16] A. W. Bassett, D. P. Rogers, J. M. Sadler, J. J. L. Scala, R. P. Wool, and J. F. Stanzione, "The effect of impurities in reactive diluents prepared from lignin model compounds on the properties of vinyl ester resins," *J. Appl. Polym. Sci.*, vol. 133, no. 45, p. 43817, Dec. 2016, doi: 10.1002/app.43817.

[17] "HELOXY^{TM} Epoxy Resin Modifiers: Ever Expanding Options," *HEXION*. https://www.hexion.com/en-us/brand/heloxy (accessed Dec. 01, 2021).

[18] C. W. Hull, "Method for production of three-dimensional objects by stereolithography," US5762856A, Jun. 09, 1998 Accessed: Nov. 29, 2021. [Online]. Available: https://patents.google.com/patent/US5762856A/en

[19] E. J. Murphy, R. E. Ansel, and J. J. Krajewski, "Investment casting utilizing patterns produced by stereolithography," US4844144A, Jul. 04, 1989 Accessed: Nov. 29, 2021. [Online]. Available: https://patents.google.com/patent/US4844144A/en

[20] X. Fernández-Francos, O. Konuray, X. Ramis, À. Serra, and S. De la Flor, "Enhancement of 3D-Printable Materials by Dual-Curing Procedures," *Materials*, vol. 14, no. 1, Art. no. 1, Jan. 2021, doi: 10.3390/ma14010107.

[21] J. A. Campbell, H. Inglis, E. Ng WeiLong, C. McKinley, and D. A. Lewis, "Morphology Control in a Dual-Cure System for Potential Applications in Additive Manufacturing," *Polymers*, vol. 11, no. 3, Art. no. 3, Mar. 2019, doi: 10.3390/polym11030420.

[22] M. Ito, H. Takamatsu, T. Taniguchi, H. Okamoto, and T. Karatsu, "Effect of Acrylic and Epoxy Hybrid Crosslinker on the Mechanical Strength of Photocurable Resin for 3D Printing," *J. Photopolym. Sci. Technol.*, vol. 34, no. 3, pp. 237–249, 2021, doi: 10.2494/photopolymer.34.237.

[23] M. Romeis and D. Drummer, "A Dyciandiamine-Based Methacrylate-Epoxy Dual-Cure Blend-System for Stereolithography," *Polymers*, vol. 13, no. 18, Art. no. 18, Jan. 2021, doi: 10.3390/polym13183139.

[24] J. R. Nowers and B. Narasimhan, "The effect of interpenetrating polymer network formation on polymerization kinetics in an epoxy-acrylate system," *Polymer*, vol. 47, no. 4, pp. 1108–1118, Feb. 2006, doi: 10.1016/j.polymer.2005.12.030.

[25] L. H. Sperling, *Interpenetrating Polymer Networks and Related Materials*. Springer Science & Business Media, 2012.

[26] M. S. Silverstein, "Interpenetrating polymer networks: So happy together?," *Polymer*, vol. 207, p. 122929, Oct. 2020, doi: 10.1016/j.polymer.2020.122929.

[27] I. Ostromislensky, "Process for Making Vitreous Polymerized Styrols and Products Obtained Thereby," US1683405A, Sep. 04, 1928 Accessed: Nov. 22, 2021. [Online]. Available: https://patents.google.com/patent/US1683405A/en?q=ostromislensky&oq=ostromislensky

[28] S. J. J. Peter and H. H. Malcolm, "Process for the production of strain-free masses from crossedlinked polymerized methylmethacrylate," US2539376A, Jan. 23, 1951 Accessed: Nov. 22, 2021. [Online]. Available: https://patents.google.com/patent/US2539376/en

[29] L. Zhang, Z. Cai, Z. Xu, Q. Yu, and Z. Liang, "Second order non-linear optical interpenetrating polymer networks based on polyurethane or poly(methyl methacrylate) and epoxy polymer," *Polym. Int.*, vol. 48, no. 6, pp. 467–472, 1999, doi: 10.1002/(SICI)1097-0126(199906)48:6<467::AID-PI171>3.0.CO;2-O.

[30] V. Simic, S. Boileau, L. Bouteiller, L. Gallez, and P. Merlin, "Gas barrier and adhesion of interpenetrating polymer networks based on poly(diurethane bismethacrylate) and different epoxy–amine networks," *Eur. Polym. J.*, vol. 38, no. 12, pp. 2449–2458, Dec. 2002, doi: 10.1016/S0014-3057(02)00164-7.

[31] W. D. Cook, F. Chen, S. K. Ooi, C. Moorhoff, and R. Knott, "Effect of curing order on the curing kinetics and morphology of bisGMA/DGEBA interpenetrating polymer networks," *Polym. Int.*, vol. 55, no. 9, pp. 1027–1039, 2006, doi: 10.1002/pi.2048.

[32] J. Wang and W. Wu, "Swelling behaviors, tensile properties and thermodynamic studies of water sorption of 2-hydroxyethyl methacrylate/epoxy methacrylate copolymeric hydrogels," *Eur. Polym. J.*, vol. 41, no. 5, pp. 1143–1151, May 2005, doi: 10.1016/j.eurpolymj.2004.11.034.

[33] J. R. Fried, *Polymer Science and Technology*. Prentice Hall Professional Technical Reference, 2003.

[34] A. W. Bassett, A. E. Honnig, J. J. La Scala, and J. F. Stanzione, "Network toughening of additively manufactured, high glass transition temperature materials via sequentially cured, interpenetrating polymers," *Polym. Int.*, vol. 70, no. 6, pp. 749–758, Jun. 2021, doi: 10.1002/pi.6091.

[35] X.-B. Ma, R. Yang, K. P. C. Sekhar, and B. Chi, "Injectable Hyaluronic Acid/Poly(γ-glutamic acid) Hydrogel with Step-by-step Tunable Properties for Soft Tissue Engineering," *Chin. J. Polym. Sci.*, vol. 39, no. 8, pp. 957–965, Aug. 2021, doi: 10.1007/s10118-021-2558-3.

[36] R. Yu *et al.*, "Three-Dimensional Printing of Shape Memory Composites with Epoxy-Acrylate Hybrid Photopolymer," *ACS Appl. Mater. Interfaces*, vol. 9, no. 2, pp. 1820–1829, Jan. 2017, doi: 10.1021/acsami.6b13531.

[37] Y. Cui, J. Yang, D. Lei, and J. Su, "3D Printing of a Dual-Curing Resin with Cationic Curable Vegetable Oil," *Ind. Eng. Chem. Res.*, vol. 59, no. 25, pp. 11381–11388, Jun. 2020, doi: 10.1021/acs.iecr.0c01507.

[38] S. C. Ligon, R. Liska, J. Stampfl, M. Gurr, and R. Mulhaupt, "Polymers for 3D Printing and Customized Additive Manufacturing," *ACS Chem. Rev.*, no. 117, pp. 10212–10290, 2017, doi: DOI: 10.1021/acs.chemrev.7b00074.

[39] N. Naseri, B. Deepa, A. P. Mathew, K. Oksman, and L. Girandon, "Nanocellulose-Based Interpenetrating Polymer Network (IPN) Hydrogels for Cartilage Applications," *Biomacromolecules*, vol. 17, no. 11, pp. 3714–3723, Nov. 2016, doi: 10.1021/acs.biomac.6b01243.

[40] B. Martin, J. Puentes, L. Wruck, and T. A. Osswald, "Degree of cure of epoxy/acrylic photopolymers: Characterization with raman spectroscopy and a modified phenomenological model," *Polym. Eng. Sci.*, vol. 58, no. 2, pp. 228–237, 2018, doi: 10.1002/pen.24550.

[41] D. R. Klein, *Organic chemistry*. Hoboken, N.J: John Wiley, 2012.

[42] D. W. van Krevelen† and K. te Nijenhuis, *Properties of Polymers: Their Correlation with Chemical Structure; their Numerical Estimation and Prediction from Additive Group Contributions*. Elsevier, 2009.

[43] A. E. Tonelli and J. Shen, *Conformations: Connecting the Chemical Structures and Material Behaviors of Polymers*. CRC Press, 2020.

[44] K. Pyrzynski, G. Nyszko, and G. E. Zaikov, *Chemical and Structure Modification of Polymers*. CRC Press, 2016.

[45] R. K. Harris, *Nuclear Magnetic Resonance Spectroscopy*. Harlow: Longman Publishing Group, 1986.

[46] F. A. Bovey, P. A. Mirau, and H. S. Gutowsky, *Nuclear Magnetic Resonance Spectroscopy*. Elsevier, 1988.

[47] J. B. Lambert, E. P. Mazzola, and C. D. Ridge, *Nuclear Magnetic Resonance Spectroscopy: An Introduction to Principles, Applications, and Experimental Methods*. John Wiley & Sons, 2019.

[48] E. D. Becker, "A BRIEF HISTORY OF NUCLEAR MAGNETIC RESONANCE," *Anal. Chem.*, vol. 65, no. 6, pp. 295A-302A, Mar. 1993, doi: 10.1021/ac00054a716.

[49] H. A. Barnes, J. F. Hutton, and K. Walters, *An Introduction to Rheology*. Elsevier, 1989.

[50] J. Mijovic, "Handbook of plastics testing technology, Vishu Shah, Wiley, New York, 1984, 493 pp. Price: $69.95," *J. Polym. Sci. Polym. Lett. Ed.*, vol. 23, no. 1, pp. 49–49, 1985, doi: 10.1002/pol.1985.130230111.

[51] A. Y. Malkin and A. I. Isayev, *Rheology: Concepts, Methods, and Applications*. Elsevier, 2017.

[52] O. Faix, "Fourier Transform Infrared Spectroscopy," in *Methods in Lignin Chemistry*, S. Y. Lin and C. W. Dence, Eds. Berlin, Heidelberg: Springer, 1992, pp. 83–109. doi: 10.1007/978-3-642-74065-7_7.

[53] J. Bates, "Fourier transform infrared spectroscopy.," *Science*, 1976, doi: 10.1126/SCIENCE.1246596.

[54] S. D.A and W. D.M, *Principles of Instrumental Analysis*, Second edition. 1980. Accessed: Nov. 16, 2021. [Online]. Available: http://gen.lib.rus.ec/book/index.php?md5=e13bf23b93a8924937ea488df0732b07

[55] D. Halliday, R. Resnick, and J. Walker, *Fundamentals of Physics*, 10th edition. Wiley, 2013.

[56] G. W. Ehrenstein, G. Riedel, and P. Trawiel, *Thermal analysis of plastics: theory and practice*. Munich; Cincinnati: Hanser ; Hanser Gardner Publications [distributor, 2004.

[57] K. P. Menard, *Dynamic Mechanical Analysis: A Practical Introduction*, 1st edition. CRC-Press, 1997.

[58] J. D. Ferry, *Viscoelastic Properties of Polymers, 3rd Edition*, 3rd edition. New York: Wiley, 1980.

[59] J. F. Stanzione, R. E. Jensen, P. J. Costanzo, and G. R. Palmese, "Characterization of room temperature ionic liquid solvent based free radical copolymerized network gels," in *International SAMPE Symposium and Exhibition (Proceedings)*, Dec. 2008, vol. 52. Accessed: Nov. 18, 2021. [Online]. Available: https://www.researchwithrowan.com/en/publications/characterization-of-room-temperature-ionic-liquid-solvent-based-f

[60] "Standard Test Method for Compressive Properties of Rigid Plastics," ASTM International, 2021. doi: 10.1520/D0695-15.

[61] L. H. Sperling, *Introduction to Physical Polymer Science*, 4th edition. Hoboken, N.J: Wiley-Interscience, 2005.

[62] D20 Committee, "Test Methods for Plane-Strain Fracture Toughness and Strain Energy Release Rate of Plastic Materials," ASTM International. doi: 10.1520/D5045-14.

[63] I. M. McAninch, J. J. La Scala, G. R. Palmese, and E. J. Robinette, "Thin film initiation of cracks for fracture toughness measurements in epoxy resins," *J. Appl. Polym. Sci.*, vol. 134, no. 1, p. app.44364, Jan. 2017, doi: 10.1002/app.44364.

[64] H. Schiefer and F. Schiefer, "Statistical Tests," in *Statistics for Engineers: An Introduction with Examples from Practice*, H. Schiefer and F. Schiefer, Eds. Wiesbaden: Springer Fachmedien, 2021, pp. 69–93. doi: 10.1007/978-3-658-32397-4_5.

[65] A. W. Bassett, A. E. Honnig, C. M. Breyta, I. C. Dunn, J. J. La Scala, and J. F. Stanzione, "Vanillin-Based Resin for Additive Manufacturing," *ACS Sustain. Chem. Eng.*, vol. 8, no. 14, pp. 5626–5635, Apr. 2020, doi: 10.1021/acssuschemeng.0c00159.

[66] J. F. S. III, J. M. Sadler, J. J. L. Scala, K. H. Reno, and R. P. Wool, "Vanillin-based resin for use in composite applications," *Green Chem.*, vol. 14, no. 8, pp. 2346–2352, Aug. 2012, doi: 10.1039/C2GC35672D.

[67] J. M. Sadler *et al.*, "Isosorbide-methacrylate as a bio-based low viscosity resin for high performance thermosetting applications," *J. Mater. Chem. A*, vol. 1, no. 40, p. 12579, 2013, doi: 10.1039/c3ta12918g.

[68] A. Bassett, "Hybrid monomers & resins for high-performance thermosetting polymers, thermoplastics, & additive manufacturing," *Theses Diss.*, Mar. 2020, [Online]. Available: https://rdw.rowan.edu/etd/2765

[69] E. D. Hernandez, A. W. Bassett, J. M. Sadler, J. J. La Scala, and J. F. Stanzione, "Synthesis and Characterization of Bio-based Epoxy Resins Derived from Vanillyl Alcohol," *ACS Sustain. Chem. Eng.*, vol. 4, no. 8, pp. 4328–4339, Aug. 2016, doi: 10.1021/acssuschemeng.6b00835.

[70] B. Abderezzak, "1 - Introduction to Hydrogen Technology," in *Introduction to Transfer Phenomena in PEM Fuel Cell*, B. Abderezzak, Ed. Elsevier, 2018, pp. 1–51. doi: 10.1016/B978-1-78548-291-5.50001-9.

[71] G. Socrates, *Infrared and Raman Characteristic Group Frequencies: Tables and Charts*. John Wiley & Sons, 2004.

[72] M. G. González, J. C. Cabanelas, and J. Baselga, "Applications of FTIR on Epoxy Resins - Identification, Monitoring the Curing Process, Phase Separation and Water Uptake," in *Infrared Spectroscopy - Materials Science, Engineering and Technology*, T. Theophanides, Ed. InTech, 2012. doi: 10.5772/36323.

[73] I. M. McAninch, G. R. Palmese, J. L. Lenhart, and J. J. La Scala, "DMA testing of epoxy resins: The importance of dimensions: DMA Testing of Epoxy Resins: The Importance of Dimensions," *Polym. Eng. Sci.*, vol. 55, no. 12, pp. 2761–2774, Dec. 2015, doi: 10.1002/pen.24167.

[74] P. J. Flory, *Principles of Polymer Chemistry*. Cornell University Press, 1953.

[75] F. R. Foulkes, *Physical chemistry for engineering and applied sciences*. Boca Raton: CRC Press, Taylor & Francis Group, 2013.

[76] "Understanding the History, Usage, and Regulation of Hexavalent Chromium [Cr(VI)]," Pantheon Enterprises.

[77] W. J. Blank, Z. A. He, and M. Picci, "CATALYSIS OF THE EPOXY-CARBOXYL REACTION." Feb. 21, 2001.

[78] I. e. Dell'Erba and R. j. j. Williams, "Homopolymerization of epoxy monomers initiated by 4-(dimethylamino)pyridine," *Polym. Eng. Sci.*, vol. 46, no. 3, pp. 351–359, 2006, doi: 10.1002/pen.20468.

[79] J. L. Han, K. H. Hsieh, and W. Y. Chiu, "Kinetics of curing reaction of epoxide catalyzed by tertiary amine," *J. Appl. Polym. Sci.*, vol. 50, no. 6, pp. 1099–1106, 1993, doi: 10.1002/app.1993.070500618.

[80] V. A. Alvarez, M. Arellano, A. Arostegui, A. F. Avila, and J. Aurrekoetxea, *Progress in Polymer Degradation and Stability Research*, 1st edition. New York: Nova Science Pub Inc, 2007.

[81] F. Hu, "Structure - Property Relationships of Furanyl Thermosetting Polymer Materials Derived from Biobased Feedstocks," 2016.

[82] C. Voirin, S. Caillol, N. V. Sadavarte, B. V. Tawade, B. Boutevin, and P. P. Wadgaonkar, "Functionalization of cardanol: towards biobased polymers and additives," *Polym. Chem.*, vol. 5, no. 9, pp. 3142–3162, 2014, doi: 10.1039/C3PY01194A.

[83] S. Chatterjee, Dhanurdhar, and L. Rokhum, "Extraction of a cardanol based liquid bio-fuel from waste natural resource and decarboxylation using a silver-based catalyst," *Renew. Sustain. Energy Rev.*, vol. 72, pp. 560–564, May 2017, doi: 10.1016/j.rser.2017.01.035.

[84] E. Can, E. Kınacı, and G. R. Palmese, "Preparation and characterization of novel vinyl ester formulations derived from cardanol," *Eur. Polym. J.*, vol. 72, pp. 129–147, Nov. 2015, doi: 10.1016/j.eurpolymj.2015.09.010.

[85] G. John, S. K. Thomas, and C. K. S. Pillai, "Cardanyl acrylate/methacrylate based cross-linked copolymers as novel supports: Synthesis and characterization," *J. Appl. Polym. Sci.*, vol. 53, no. 11, pp. 1415–1423, 1994, doi: 10.1002/app.1994.070531103.

[86] S. Agarwal, V. Choudhary, and I. K. Varma, "Preparation and characterization of copolymers from methyl methacrylate and cardanyl methacrylate," *Angew. Makromol. Chem.*, vol. 248, no. 1, pp. 95–104, 1997, doi: 10.1002/apmc.1997.052480106.

[87] W. S. J. Li *et al.*, "Cardanol-based polymer latex by radical aqueous miniemulsion polymerization," *Polym. Chem.*, vol. 9, no. 18, pp. 2468–2477, May 2018, doi: 10.1039/C8PY00167G.

[88] R. Bhoi, D. Singh, and S. Mahajani, "Investigation of mass transfer limitations in simultaneous esterification and transesterification of triglycerides using a heterogeneous catalyst," *React. Chem. Eng.*, vol. 2, no. 5, pp. 740–753, Oct. 2017, doi: 10.1039/C6RE00218H.

[89] Y. Ma, Y. Liu, H. Su, L. Wang, and J. Zhang, "Relationship between hydrogen bond and viscosity for a series of pyridinium ionic liquids: Molecular dynamics and quantum chemistry," *J. Mol. Liq.*, vol. 255, pp. 176–184, Apr. 2018, doi: 10.1016/j.molliq.2018.01.121.

[90] J. A. Ramos, N. Pagani, C. C. Riccardi, J. Borrajo, S. N. Goyanes, and I. Mondragon, "Cure kinetics and shrinkage model for epoxy-amine systems," *Polymer*, vol. 46, no. 10, pp. 3323–3328, Apr. 2005, doi: 10.1016/j.polymer.2005.02.069.

[91] H. M. Fadda, M. Khanna, J. C. Santos, D. Osman, S. Gaisford, and A. W. Basit, "The use of dynamic mechanical analysis (DMA) to evaluate plasticization of acrylic polymer films under simulated gastrointestinal conditions," *Eur. J. Pharm. Biopharm.*, vol. 76, no. 3, pp. 493–497, Nov. 2010, doi: 10.1016/j.ejpb.2010.08.007.

[92] C. E. C. Jr and R. B. Seymour, *Structure—Property Relationships in Polymers*. Springer Science & Business Media, 2012.

[93] D. L. Safranski and K. Gall, "Effect of chemical structure and crosslinking density on the thermo-mechanical properties and toughness of (meth)acrylate shape memory polymer networks," *Polymer*, vol. 49, no. 20, pp. 4446–4455, Sep. 2008, doi: 10.1016/j.polymer.2008.07.060.

[94] I. M. Barszczewska-Rybarek, A. Korytkowska-Wałach, M. Kurcok, G. Chladek, and J. Kasperski, "DMA analysis of the structure of crosslinked poly(methyl methacrylate)s," *Acta Bioeng. Biomech.*, vol. Vol. 19, no. nr 1, 2017, doi: 10.5277/ABB-00590-2016-01.

[95] I. McAninch, G. Palmese, J. Lenhart, and J. La Scala, "Characterization of epoxies cured with bimodal blends of polyetheramines," *J. Appl. Polym. Sci.*, vol. 130, Nov. 2013, doi: 10.1002/app.39322.

[96] K. Sweet, "Epoxy-functional thermoplastic copolymers and their incorporation into thermosetting resins," *Theses Diss.*, Sep. 2020, [Online]. Available: https://rdw.rowan.edu/etd/2843

[97] W. G. Perkins, "Polymer toughness and impact resistance," *Polym. Eng. Sci.*, vol. 39, no. 12, pp. 2445–2460, 1999, doi: 10.1002/pen.11632.

[98] M. H. Al-Saleh and M. R. Irshidat, "Effect of viscosity reducing agent on the properties of CNT/epoxy nanocomposites," *J. Polym. Eng.*, vol. 36, no. 4, pp. 407–412, May 2016, doi: 10.1515/polyeng-2015-0245.

[99] E. Urbaczewski-Espuche, J. Galy, J.-F. Gerard, J.-P. Pascault, and H. Sautereau, "Influence of chain flexibility and crosslink density on mechanical properties of epoxy/amine networks," *Polym. Eng. Sci.*, vol. 31, no. 22, pp. 1572–1580, 1991, doi: 10.1002/pen.760312204.

[100] H. Quan, T. Zhang, H. Xu, S. Luo, J. Nie, and X. Zhu, "Photo-curing 3D printing technique and its challenges," *Bioact. Mater.*, vol. 5, no. 1, pp. 110–115, Mar. 2020, doi: 10.1016/j.bioactmat.2019.12.003.

[101] G. Wisanrakkit and J. Gillham, "Continuous heating transformation (CHT) cure diagram of an aromatic amine/epoxy system at constant heating rates," 1991, doi: 10.1002/APP.1991.070420911.

[102] F. Hu, J. J. La Scala, J. M. Sadler, and G. R. Palmese, "Synthesis and Characterization of Thermosetting Furan-Based Epoxy Systems," *Macromolecules*, vol. 47, no. 10, pp. 3332–3342, May 2014, doi: 10.1021/ma500687t.

[103] A. Chatterjee, "Thermal degradation analysis of thermoset resins," *J. Appl. Polym. Sci.*, vol. 114, no. 3, pp. 1417–1425, 2009, doi: 10.1002/app.30664.

[104] J. F. Stanzione, K. E. Strawhecker, and R. P. Wool, "Observing the twinkling fractal nature of the glass transition," *J. Non-Cryst. Solids*, vol. 357, no. 2, pp. 311–319, Jan. 2011, doi: 10.1016/j.jnoncrysol.2010.06.041.

[105] A. R. Kannurpatti, J. W. Anseth, and C. N. Bowman, "A study of the evolution of mechanical properties and structural heterogeneity of polymer networks formed by photopolymerizations of multifunctional (meth)acrylates," *Polymer*, vol. 39, no. 12, pp. 2507–2513, Jan. 1998, doi: 10.1016/S0032-3861(97)00585-5.

[106] M. A. Downey and L. T. Drzal, "Toughening of aromatic epoxy via aliphatic epoxy copolymers," *Polymer*, vol. 55, no. 26, pp. 6658–6663, Dec. 2014, doi: 10.1016/j.polymer.2014.10.052.

[107] C.-H. Zhang, H.-G. Wei, Y.-Y. Liu, H.-F. Tan, and Z. Guo, "Enhanced toughness and shape memory behaviors of toughed epoxy resin," *High Perform. Polym.*, vol. 24, no. 8, pp. 702–709, Dec. 2012, doi: 10.1177/0954008312449846.

[108] D. C. Phillips, J. M. Scott, and M. Jones, "Crack propagation in an amine-cured epoxide resin," *J. Mater. Sci.*, vol. 13, no. 2, pp. 311–322, Feb. 1978, doi: 10.1007/BF00647775.

[109] S. Yamini and R. J. Young, "The mechanical properties of epoxy resins," *J. Mater. Sci.*, vol. 15, no. 7, pp. 1814–1822, Jul. 1980, doi: 10.1007/BF00550602.

[110] P. Phukan, "Iodine as an Extremely Powerful Catalyst for the Acetylation of Alcohols under Solvent-Free Conditions," *Cheminform*, vol. 35, Jun. 2004, doi: 10.1002/chin.200438059.

[111] S. Ko, M. N. V. Sastry, C. Lin, and C.-F. Yao, "Molecular iodine-catalyzed one-pot synthesis of 4-substituted-1,4-dihydropyridine derivatives via Hantzsch reaction," *Tetrahedron Lett.*, vol. 46, no. 34, pp. 5771–5774, Aug. 2005, doi: 10.1016/j.tetlet.2005.05.148.

[112] S. N. Khot *et al.*, "Development and application of triglyceride-based polymers and composites," *J. Appl. Polym. Sci.*, vol. 82, no. 3, pp. 703–723, 2001, doi: 10.1002/app.1897.

[113] S. Araujo *et al.*, "A structural interpretation of the two components governing the kinetic fragility from the example of interpenetrated polymer networks," *J. Polym. Sci. Part B Polym. Phys.*, vol. 56, no. 20, pp. 1393–1403, 2018, doi: 10.1002/polb.24722.

[114] B. Sibaja, C. P. Matheus, R. B. Mendez, J. R. Vega-Baudrit, and M. L. Auad, "Synthesis and Characterization of Interpenetrating Polymer Networks (IPNs) from Acrylated Soybean Oil and α-Resorcylic Acid: Part 1. Kinetics of Network Formation," *J. Renew. Mater.*, vol. 5, no. 3–4, pp. 231–240, Jul. 2017, doi: 10.7569/JRM.2017.634113.

[115] C. Dall'Argine, A. Hochwallner, N. Klikovits, R. Liska, J. Stampf, and M. Sangermano, "Hot-Lithography SLA-3D Printing of Epoxy Resin," *Macromol. Mater. Eng.*, vol. 305, no. 10, p. 2000325, Oct. 2020, doi: 10.1002/mame.202000325.

[116] W. Bras *et al.*, "Simultaneous studies of reaction kinetics and structure development in polymer processing," *Science*, vol. 267, no. 5200, pp. 996–999, Feb. 1995, doi: 10.1126/science.267.5200.996.

[117] B. Suthar, H. X. Xiao, D. Klempner, and K. C. Frisch, "A review of kinetic studies on the formation of interpenetrating polymer networks," *Polym. Adv. Technol.*, vol. 7, no. 4, 1996, doi: 10.1002/(sici)1099-1581(199604)7:43.0.co;2-a.

Appendix A

Values for *t*-Distribution

Table A1

Values of the t-distribution [64]
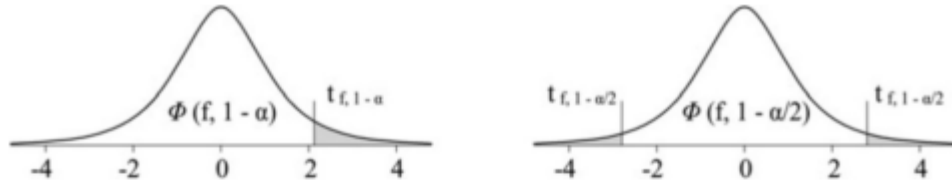
	Two-sided confidence interval						
	0.8	0.9	0.95	0.98	0.99	0.998	0.999
	One-sided confidence interval						
f	0.90	0.95	0.975	0.99	0.995	0.999	0.9995
1	3.078	6.314	12.706	31.821	63.657	318.309	636.578
2	1.886	2.920	4.303	6.965	9.925	22.327	31.600
3	1.638	2.353	3.182	4.541	5.841	10.215	12.924
4	1.533	2.132	2.776	3.747	4.604	7.173	8.610
5	1.476	2.015	2.571	3.365	4.032	5.893	6.869
6	1.440	1.943	2.447	3.143	3.707	5.208	5.959
7	1.415	1.895	2.365	2.998	3.499	4.785	5.408
8	1.397	1.860	2.306	2.896	3.355	4.501	5.041
9	1.383	1.833	2.262	2.821	3.250	4.297	4.781
10	1.372	1.812	2.228	2.764	3.169	4.144	4.587
11	1.363	1.796	2.201	2.718	3.106	4.025	4.437
12	1.356	1.782	2.179	2.681	3.055	3.930	4.318
13	1.350	1.771	2.160	2.650	3.012	3.852	4.221
14	1.345	1.761	2.145	2.624	2.977	3.787	4.140
15	1.341	1.753	2.131	2.602	2.947	3.733	4.073
16	1.337	1.746	2.120	2.583	2.921	3.686	4.015
17	1.333	1.740	2.110	2.567	2.898	3.646	3.965
18	1.330	1.734	2.101	2.552	2.878	3.610	3.922
19	1.328	1.729	2.093	2.539	2.861	3.579	3.883
20	1.325	1.725	2.086	2.528	2.845	3.552	3.850

Degree of freedom $f = n - 1$

¹H-NMR Spectra

Figure B1

¹H-NMR spectrum of PMEM828 Week 2 of Stability Study at Room Temperature
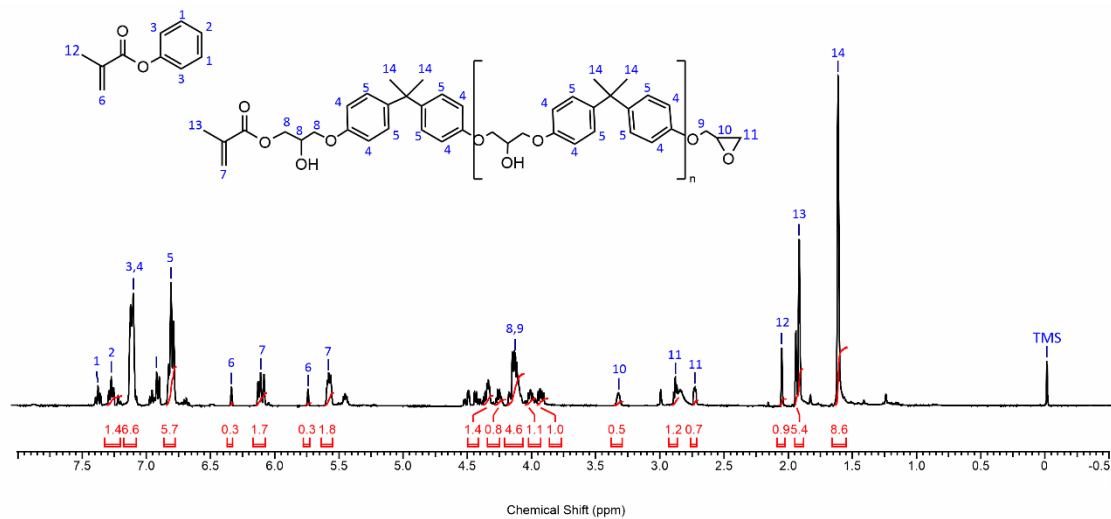

Chemical Shift (ppm)

Figure B2

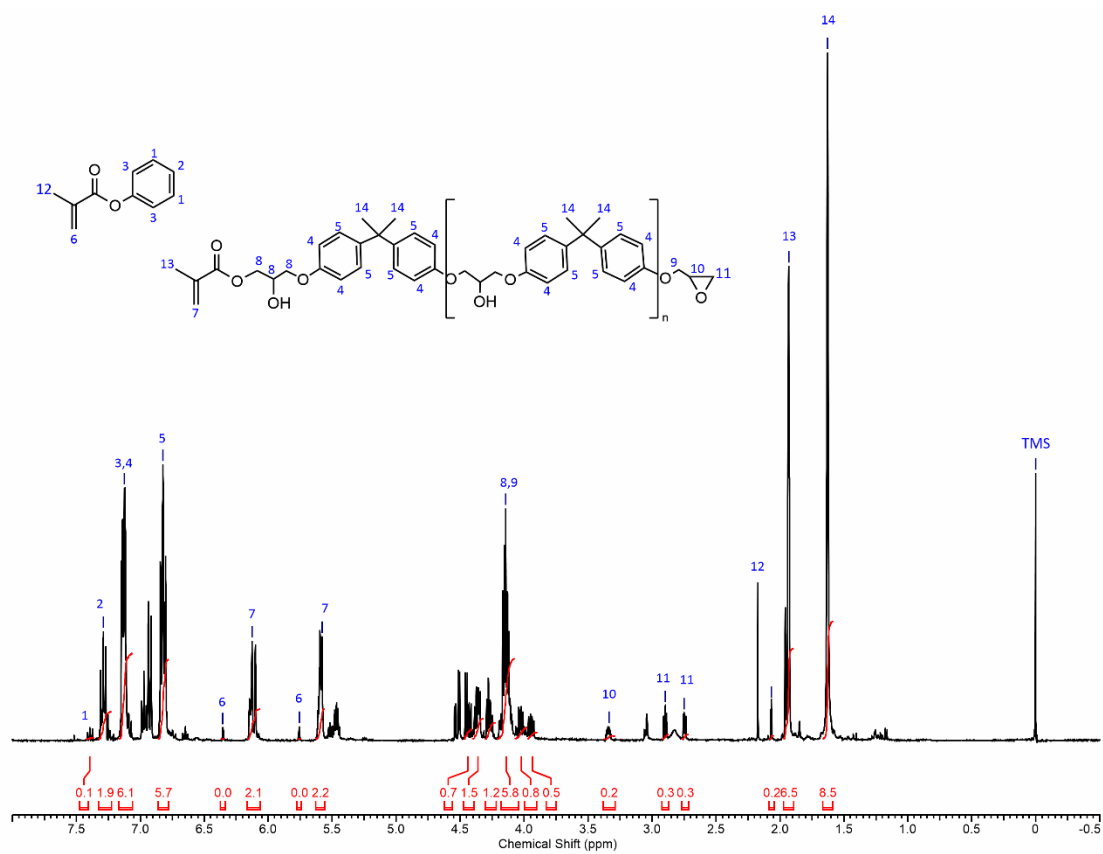*¹H-NMR spectrum of PMEM828 Week 4 of Stability Study at Room Temperature*

Figure B3

¹H-NMR spectrum of PMEM828 Without AMC-2 Week 2 of Stability Study at Room
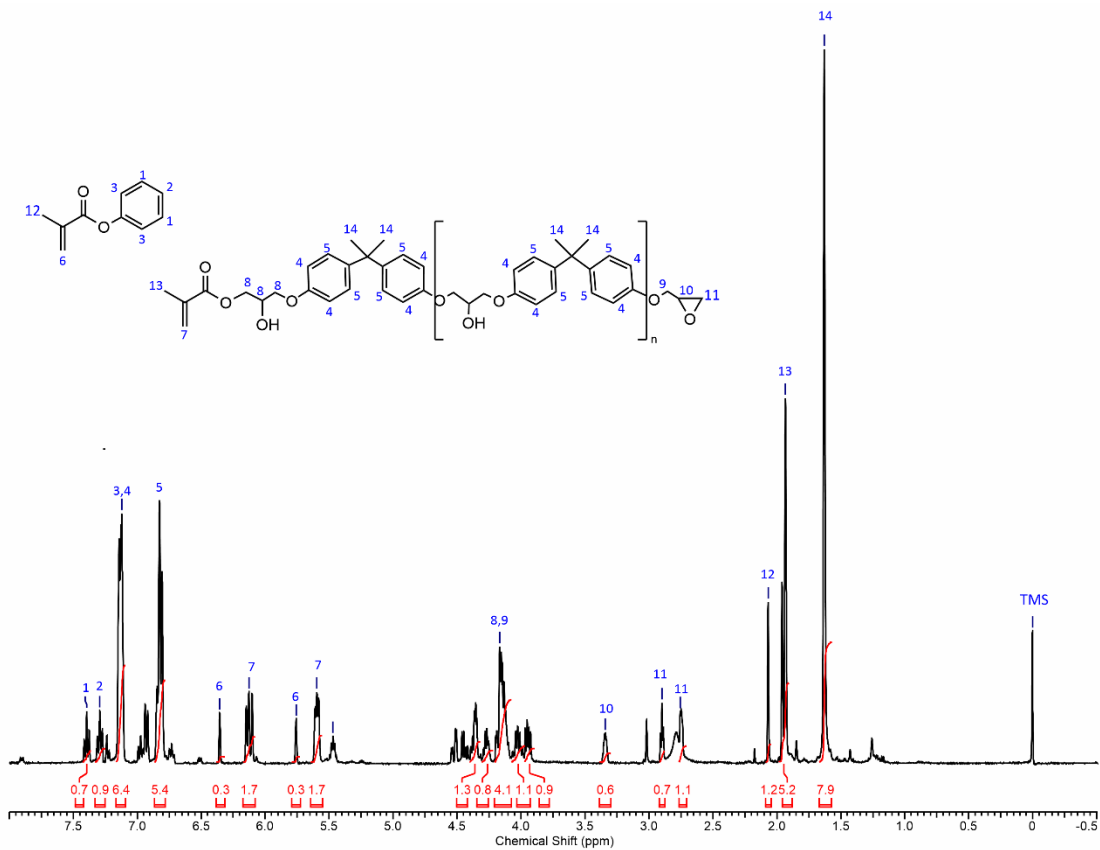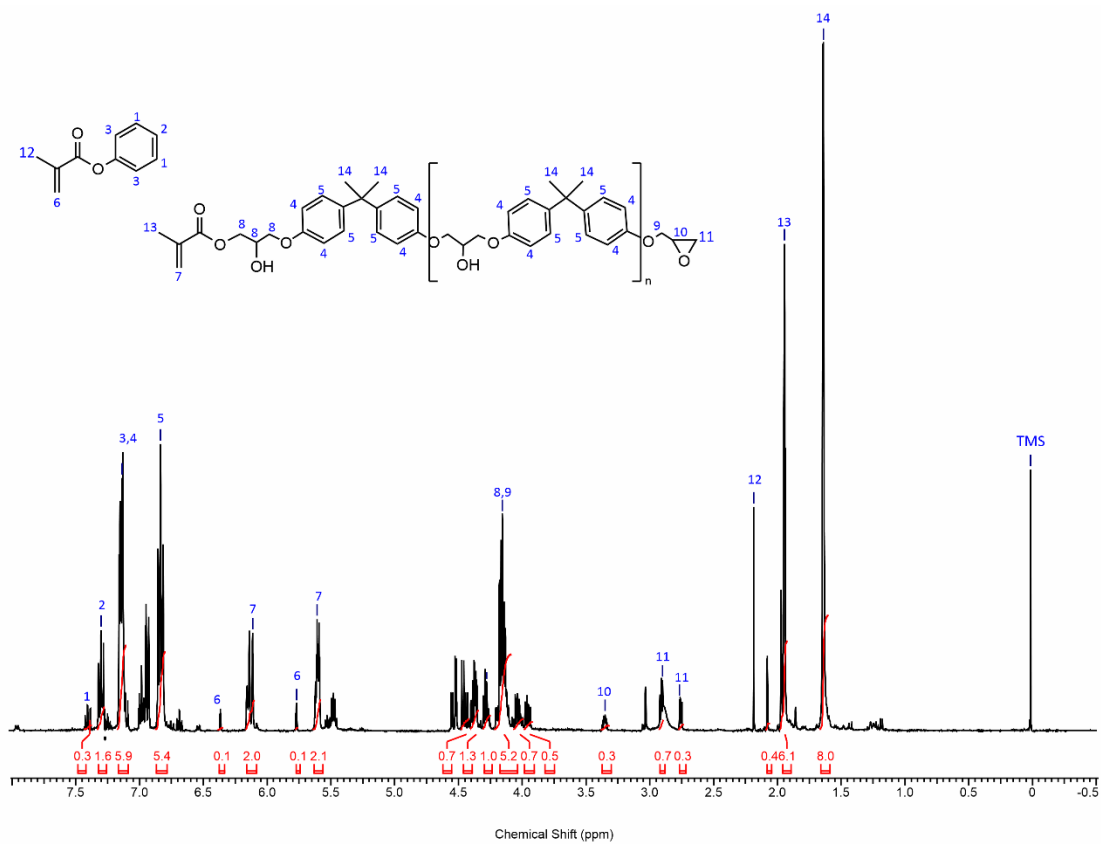
Temperature

Figure B4

¹H-NMR spectrum of PMEM828 Without AMC-2 Week 4 of Stability Study at Room

Temperature

TGA Thermograms

Figure C1

TGA Thermograms and Respective 1ˢᵗ Derivative of PMEM828 Catalyzed With and Without AMC-2 in Air
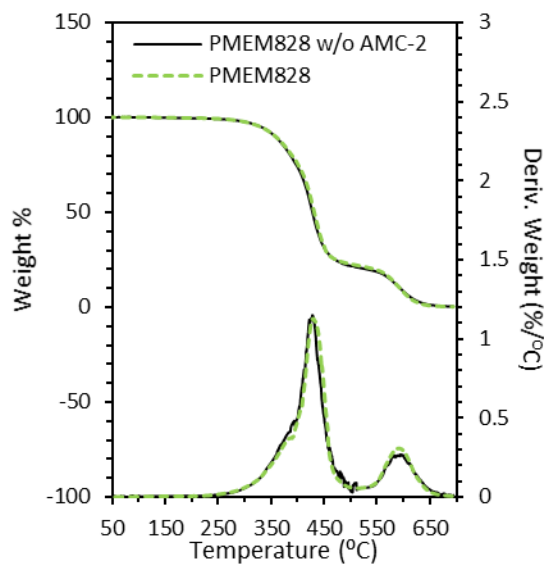

Table C1

Thermogravimetric Analysis Data of PMEM828 Catalyzed With and Without AMC-2 in Air

Sample	IDT (°C)	$T_{50\%}$ (°C)	T_{max} (°C)	Char Content (%)
PMEM828	330 ± 1	431	428 ± 1	0.27 ± 0.02
PMEM828 w/o AMC-2	329 ± 3	427 ± 1	427 ± 1	0.33 ± 0.01

Figure C2

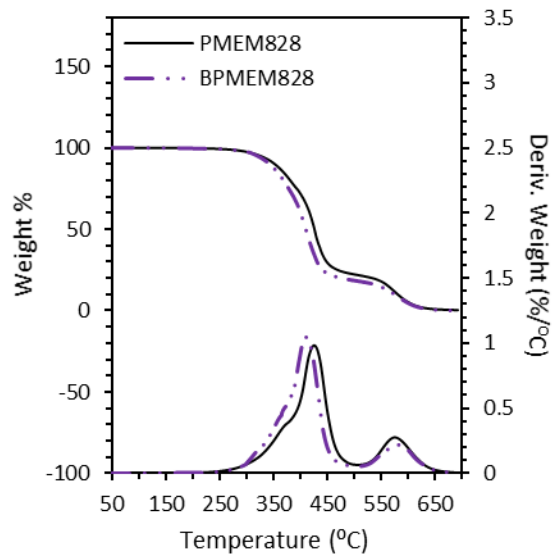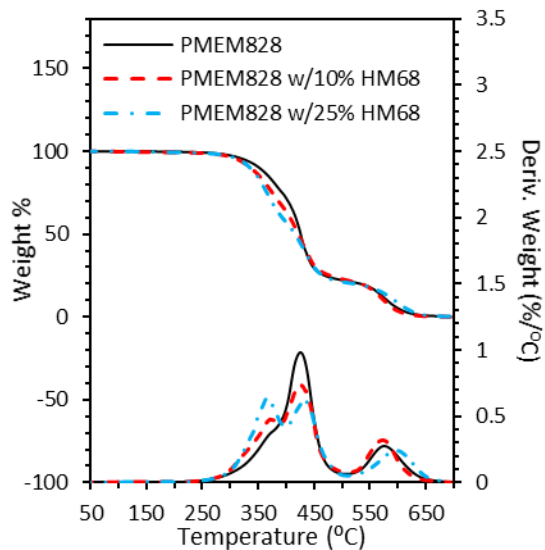*TGA Thermograms and Respective 1ˢᵗ Derivative of PMEM828 and BPMEM828 in Air*

Table C2

Thermogravimetric Analysis Data of PMEM828 and BPMEM828 in Air

Sample	IDT (°C)	$T_{50\%}$ (°C)	T_{max} (°C)	Char Content (%)
PMEM828	324 ± 8	424 ± 8	422 ± 7	0.4 ± 0.2
BPMEM828	317 ± 4	410 ± 2	412 ± 5	0.7 ± 0.8

Figure C3

TGA Thermograms and Respective 1ˢᵗ Derivative of All IPNs With HM68 in Air

Table C3

Thermogravimetric Analysis Data of IPNs With HM68 in Air

Sample	IDT (°C)	$T_{50\%}$ (°C)	T_{max} (°C)	T_{max2} (°C)	Char Content (%)
PMEM828	324 ± 8	424 ± 8	422 ± 7	-	0.4 ± 0.2
PMEM828 w/ 10% HM68	319 ± 5	423 ± 1	373 ± 2	428 ± 3	0.1 ± 0.1
PMEM828 w/ 25% HM68	311 ± 8	416 ± 1	365 ± 4	430 ± 3	0.3 ± 0.1

Appendix D

Additional DMA Data

Table D1

Additional Viscoelastic Data of PMEM828 With and Without AMC-2

Sample	Rubbery E′ (MPa)	Rubbery T (°C)
PMEM828	29.8 ± 0.8	171 ± 1
PMEM828 w/o AMC-2	23.2 ± 0.6	169 ± 2

Table D2

Additional Viscoelastic Data of PMEM828 and BPMEM828

Sample	Rubbery E′ (MPa)	Rubbery T (°C)
PMEM828	26.8 ± 3.0	169 ± 5
BPMEM828	16.0 ± 1.0	178 ± 1

Table D3

Additional Viscoelastic Data of All IPNs With HM68

Sample	Rubbery E′ (MPa)	Rubbery T (°C)
PMEM828	26.8 ± 3.0	169 ± 5
PMEM828 w/ 10% HM68	20.5 ± 0.9	160 ± 7
PMEM828 w/ 25% HM68	17.5 ± 1.3	163 ± 10

Appendix E

List of Acronyms, Abbreviations, and Symbols

3D printing	Three-dimensional printing
AM	Additive manufacturing
BPM	Tertbutyl Methacrylate
CT	Compact Tension
DMA	Dynamic mechanical analysis
DMAP	4-dimethylaminopyridine
DSC	Differential scanning calorimetry
E'	Storage Modulus
E''	Loss Modulus
EM828	Partially methacrylate diglycidyl ether of bisphenol A
Epon828	Diglycidyl ether of bisphenol A
FC	Form cure
FTIR	Fourier transform infrared
G_{1C}	Critical strain energy release rate
GMA	Glycidyl methacrylate
HM	HELOXY^{TM} modifier
IDT	Initial decomposition temperature at 5% weight loss
IPA	Isopropyl Alcohol
IPN	Interpenetrating polymer network
K_{1C}	Critical-stress-intensity factor

M_c	Molecular weight between crosslinks
N_2	Nitrogen
NMR	Nuclear magnetic resonance
PC	Post-cured
SENB	Single edge notched bend
SLA	Stereolithography
T_g	Glass transition temperature
Tan δ	Tan delta
TGA	Thermogravimetric Analysis
TMS	Tetramethylsilane
TPO	Diphenyl(2,4,6-trimethylbenzoyl) phosphine oxide
VPP	Vat photopolymerization
ρ	density